PB-230 312

HEAT TRANSFER AND FRICTION LOSS PERFORMANCE OF HEATED PERFORATED FLAT PLATES

Wen-Jei Yang, et al

Michigan University
Ann Arbor, Michigan

December 1971

DISTRIBUTED BY:

NTIS

National Technical Information Service
U. S. DEPARTMENT OF COMMERCE
5285 Port Royal Road, Springfield Va. 22151

PB 230 312

FINAL REPORT

HEAT TRANSFER AND FRICTION LOSS PERFORMANCE OF HEATED PERFORATED FLAT PLATES

December 1971

prepared by

Wen-Jei Yang
J. A. Clark
I. C. Macedo
K. H. Choy
J. W. Ou
C. Y. Liang

Prepared for
Office of Air Programs
Environmental Protection Agency
Ann Arbor, Michigan 48105

Reproduced by
NATIONAL TECHNICAL
INFORMATION SERVICE
U S Department of Commerce
Springfield VA 22151

Department of Mechanical Engineering
The University of Michigan
Ann Arbor, Michigan 48104

ABSTRACT

A large scale modelling technique is developed to examine the effects of perforation geometry on the heat transfer and friction loss performance of compact heat exchangers consisting of the plate-perforated rectangular fin surfaces. The technique can also be used to determine an optimum perforation geometry and to interpret test data from compact heat exchangers. The test core consists of an electrically heated metal plate and several unheated, parallel dummy plates forming rectangular flow channels. Both test and dummy plates were identically perforated in either a staggered round-hole pattern or a staggered oval-slotted pattern. The cores were tested in a subsonic wind tunnel designed specifically for testing automobile radiators, environmental system condensers, and air-water heat exchangers. Both the plate surface porosity and the core frontal porosity were varied. The Reynolds numbers ranged from laminar to turbulent flow. The heat transfer factor (j), friction factor (f) and their ratio (f/j) for a single plate-channel system are obtained as functions of the Reynolds number, the plate surface porosity and the core frontal porosity. These results are compared with average data taken from a compact plate - fin heat exchanger having the same geometric scaling factors. The data from these two systems are shown to be in satisfactory agreement when represented by appropriate geometric, dynamic and thermodynamic similarity parameters. It is shown that the f/j ratio for a perforated plate of very low surface porosity is higher than that of a solid plate. For the perforation geometry of both the round hole and slotted patterns, the heat transfer and friction behavior seem to be most favorable for the plate surface porosities between 12 and 20 percent.

INTRODUCTION

In recent years, a number of reports have been published on the heat transfer and friction loss performance of compact heat exchangers. Among them, the most notable one is the work of Kays and London [1]. The compactness refers to high area density surfaces and can be usually realized by the use of fins. Since this type of heat exchangers deals with low density fluids such as gases, the cost of friction per mass unit of flow is substantial and thus the friction characteristics of the surface is as important as the heat transfer behavior.

Among all the extended surfaces of both the plate-fin and tubular types, the use of the louvered-plate-fin surface has been favored by some applications, not only because of its high area-to-volume ratio but also for higher heat transfer coefficient resulting from boundary layer interruptions. However, the high heat transfer performance is accompanied by high pressure loss. The perforated-plate-fin surface has the heat transfer and friction loss performance comparable to the louvred-plate-fin surface. Both surfaces have advantages as well as disadvantages. However, the compactness of the louvered fin type heat exchangers is limited by the geometry of the louvers. If very high area density or compactness is required such as for the condenser in the low-pollution potential Rankine-cycle steam power plant for automobile applications, perhaps only plain-plate-fin surface or perforated-plate-fin surface can serve the purpose. The superiority of the latter surface over the former has been demonstrated in Reference [1].

Recently, very compact, plate-perforated fin heat exchangers were tested for the heat transfer and friction loss performance [2]. Results for ten cores

of two perforated fin patterns, round circle and slotted patterns, indicate substantial differences in the performance, depending on the pattern as well as the plate surface porosity. However, the test results do not indicate why one surface is better than another. More importantly, the pattern and plate surface porosity which may yield the optimum performance cannot be determined without substantial expense and effort. It was decided therefore, to develop a technique for examining the effects of perforation geometry on the heat transfer and friction loss performance of perforated-plate-fin type compact heat exchangers and to determine the perforation geometry which yields the optimum performance. The working principle for this technique has been that the tests should be relatively simple and quick to carry out, since it would be necessary to examine the performance of a large number of different surfaces. In order to achieve fine detail, a large scale was chosen, with individual units approximately ten times larger than those fins used in compact condensers. The perforated test and dummy plates have been arranged in parallel to form a test core with rectangular channels for the flow of cooling air. The test plate can be considered a section of rectangular fins attached between two plates. In this report, the large scale technique is described and its relevance to an understanding of the test data of the plate-perforated rectangular fin heat exchangers discussed.

The technique is used for testing the heat transfer and friction loss perofrmance of the round hole and slotted plates. Results are compared with those of the plate-fin heat exchangers of the same perforation geometry. Semi-emperical equations are developed based on the infinite slot model for correlating the test results.

EXPERIMENTAL APPARATUS AND PROCEDURE

The experimental setup used to investigate the heat transfer and friction loss performance of perforated plates consisted of a heat exchanger test core mounted in a subsonic wind tunnel.

The heat exchanger test core, as schematically illustrated in Fig. 1, was constructed for large scale testing of the plate-rectangular fin surface shown in Fig. 2. It consisted of an electrically heated aluminum plate and several dummy plates made of fiberglass. All the plates were 1/32-inch thick (t) and identically perforated with round holes of a staggered arrangement. The number and diameter of the round holes determine the surface porosity or percent open area. The plates were arranged in parallel with the test plate as the center piece. Wood slabs were used to space the plates for air flow passages. The thickness of the wood slabs was varied to have different values of the plate thickness-to-spacing ratio or the frontal porosity. The plates and wood slabs were stacked together by 1/4-inch bolts. The total number of the plates and slabs determines the frontal areas of the test core: 6-inch width, w, by 6-inch or 4-inch height. Thus, the w/t ratio for the test core is 192. This may be compared with 79, the w/t ratio, for a fin of 0.004-inch thickness and 0.320-inch height, which is that of a prototype heat exchanger used as a reference, Fig. 2. For both systems, the ratios were large enough to warrant the neglect of side effects on the flows through the channels. The test plate was 6 inches long in the flow direction.

Aluminum was selected as the material for the test plate for several reasons: (i) its high thermal conductivity which tends to produce a uniform temperature distribution, (ii) sufficiently high electric resistance to warrant electrical heating, (iii) easy for perforation by drilling or punching, and (iv) the Garrett condenser for low-pollution potential steam engine is made

of the same material. Fiberglass was used as the dummy plates. Only the test plate was heated for the investigation of convective heat transfer to the air, while the unheated dummy plates were used for the study of friction loss of air flow over the plates.

The wind tunnel consisted of a contraction section, test section, diffuser, fan, and discharge ducting as shown in Fig. 3. It was originally designed with the capability for testing both scale models and full size automotive radiators and condensers over a range of vehicle speeds and air-side pressure drops appropriate to automotive application.

Three flow control methods may be used to meet the air flow requirements of the tunnel: (1) a 2:1 fan speed reduction by means of switching the voltage of the electric motor which reduces fan air flow by this same ratio; (2) variable inlet guide vane geometry capable of producing a continuous variation in fan air flow from 15% to 100% of maximum air flow; and (3) a bypass around the test section which can produce a continuous variation in test section air flow from 10 to 100% of maximum test section air flow. The change in fan speed and the inlet guide van geometry produce changes in fan characteristics while the tunnel bypass alters the total system flow characteristic to vary the test section air flow. The bypass also allows the fan to operate in a surge-free region at all times. The bypass is accomplished by constructing the contraction section and the test section as a single unit and then translating this unit forward relative to the fixed diffuser and fan.

In order to obtain the information on the uniformity of the air flow in the test section of the wind tunnel, horizontal and vertical Pitot tube traverses were made in a plane normal to the tunnel longitudial axis and located near

the middle of the test section. The traverses were made at 3-inch intervals except near the walls where the spacing was reduced to 1.5 and then to 0.25 inches from the walls. Using the velocity at the center of the tunnel as the reference velocity (at 77.1 ft/sec), it was found that at a distance of 1.5 inches velocities were generally within 3% of the reference velocity, while at all distances 3 inches or further from the walls velocities were within 1.5% of the reference value. These results indicated the uniformity of air flow in the test section of the wind tunnel.

The test core was installed in the test section of the wind tunnel. Electric power was supplied to the test plate through cables from a low-voltage M-G power supply (36 Kw, 0-12v, 0-3000 amp). In order to insure flexibility of operation, the power source and the test plate were arranged in series with a stainless steel pipe to form a power supply loop, as illustrated in Fig. 4. The pipe which was internally cooled by water from municipal supply was designed to dissipate excess electric power. By varying the length of the pipe and/or by adjusting the water flow rate through the pipe, the electric power dissipated in the test plate was adjusted so that the plate surface temperature was set in a desired range. Because of relatively low electrical resistance, only fraction of electric power from the power supply was consumed by the aluminum test plate. Therefore, the stainless pipe became a power consuming section. A shunt of known electrical resistance was installed in the power supply loop. The voltage drops across the shunt and the test plate (only the portion that was exposed to the air stream) were measured by a Weston Model 622 Millivoltmeter. The electric power that dissipated in the test section was transmitted to the air stream. The portion of the test plate which protuded out of the baffle and the copper connectors which were used to bridge the power supply cables to the test plate

were well insulated with fiberglas to prevent heat loss to the ambient.

Since the frontal area of all of the test cores was considerably less than the wind tunnel test section area, the cores were mounted on a support which was fixed to the bottom of the test section, as depicted in Fig. 5. Baffles of constant area section were installed immediately upstream as well as downstream of the core. A bellmouth in the inlet end of the constant area section was used to insure proper inlet flow conditions. Sealing was used around the core-baffle joint and also the baffle-test section wall joint to insure that all of the airflow which entered the constant area section flowed through the core.

Two pitot tubes were inserted into the constant area sections, one at upstream and the other at downstream. The Pitot tubes were connected to a Meriam micro-type manometer to read four pressure differences: total to static pressure differences at both upstream and downstream and total to total and static to static pressure differences between upstream and downstream. The air velocities at the inlet and exit of the test core and the static, dynamic and total friction losses in the test core were evaluated from these pressure measurements. Temperatures were measured by copper-constantan thermocouples and read on a L & N 8662 precision potentiometer. The inlet air temperature was read by a thermocouple located near the tip of the upstream Pitot tube. Three thermocouples were mounted on the test plate surface at 1/2" back from the downstream edge as shown in Figure 1. One was on the center line of the test plate and the other two were 2 inches from the center one on each side. The tips of these thermocouples, electrically insulated from the test plate by very thin mica films, were clamped tightly on the plate surface. The readings of these three thermocouples were very close because of high thermal conductivity of the test plate (aluminum). Their

arithmatic average was used as the plate surface temperature. Three copper rods were erected vertically at 5-inch distance downstream from the edge of the test plate, one at the center of the constant area section and the other two at 1.5-inch apart on each side. Four thermocouples were mounted on the rods, two on the center rod and one each on the other two rods. They measured the distribution of the outlet air temperatures at four different vertical locations downstream from the test plate, as indicated in Fig. 1. The first thermocouple (on the left rod) was lined up with test plate, while the location of the other three thermocouples was varied according to plate spacing. The second and third thermocouples (on the center rod) were located at two different vertical positions in between the test plate and the neighboring dummy plate. The fourth thermocouple (on the right rod) which was installed slightly below the dummy plate almost always read the temperature of the inlet air or slightly above it. The integrated mean value of the measured temperature distribution was employed as the average outlet temperature of the air streams from the channels heated by the test plate.

The desired air velocity through the test section was set by means of adjusting bypass opennng. The electrical power supply was adjusted to hold the plate surface temperature at about 200°F. When steady state conditions had been established, air and surface temperatures, pressure drops and voltages were recorded.

TEST RESULTS

The electric power dissipated as heat in the test plate is equal to the product of the voltage drop across the test plate and the current flowing in the power supply loop. The heat was then transmitted to the air stream in the channels wetting the test plate by convection (at the rate of q Btu/hr). Therefore, the heat transfer coefficient between the test plate and the air stream, h can be evaluated using the equation $q=hA(T_s-T_a)$, where A is the heat transfer area, T_s is the plate surface temperature and T_a is the mean bulk temperature (average of the inlet and the outlet) of the air stream. As a result of convective heat transfer, the enthalpy of the air streams has increased by $mC_p(T_{ae}-T_{ai})$, where m is the flow rate of the air streams in the channels wetting the test plate, C_p is the specific heat of the air and T_{ai} and T_{ae} are the air temperatures at the inlet and exit, respectively. Good agreement between the enthalpy change of the air stream and the power input was obtained in the tests.

The heat transfer performance was expressed by the heat transfer factor j, which is defined as

$$j = \frac{h}{GC_p} P_r^{2/3} \qquad (1)$$

where G is the mass velocity, i.e., the product of the density ρ and the flow velocity, C_p is the specific heat at constant pressure, and P_r is the Prandtl number. All physical properties of the air were evaluated at the mean bulk temperature. The flow velocity is calculated using the Bernoulli's equation

$$V = \left[2g_c(\Delta P_{T-S})_i/\rho\right]^{1/2} \qquad (2)$$

where $(\Delta P_{T-S})_i$ is the total-to-static pressure difference measured by the upstream pitot tube and g_c is the conversion factor. The flow velocity is not different appreciably from that based on $(\Delta P_{T-S})_e$ measured by the downstream pitot tube.

The Reynolds number which indicates flow conditions in the test core is defined based on the hydraulic radius r_h of the flow channels in the core as

$$Re = \frac{4 r_h G}{\mu} \qquad (3)$$

where μ is the absolute viscosity. The hydraulic radius is defined as four times the flow cross-sectional area A_c divided by the wetted perimeter. For the present system, it is equal to $\frac{wb}{2(w+b)}$ where b is the plate spacing and w is the width of the channel.

The friction factor f is defined based on the static pressure drop across the test core ΔP_{s-s} as

$$f = \frac{\Delta P_{s-s}}{4G^2/(2g_c \rho r_h)} \qquad (4)$$

Both the j and f factors are functions of the frontal porosity of the test core, the plate surface porosity (percent open area) and the Reynolds number.

The frontal porosity σ_F is the ratio of the free flow to frontal area. It is related to the ratio of the plate thickness to spacing ϵ $(= t/b)$ as

$$\sigma_F = \frac{1}{1+\epsilon} \qquad (5)$$

For the perforation geometry in Fig. 6, the plate surface porosity σ_s can be expressed as

$$\sigma_s = \frac{\pi}{2\sqrt{3}} \left(\frac{d}{l}\right)^2 \qquad (6)$$

for the round hole pattern, a staggered arrangement, where d is the hole diameter and l is the center-to center distance between two adjacent holes. It is a function of only one dimensionless parameter d/l. In the case of the oval slotted pattern,

$$\sigma_s = \frac{\frac{\pi}{4} d_s^2 + d_s (w_s - d_s)}{P_t P_l} = \frac{\frac{\pi}{4} + \left(\frac{w_s}{d_s} - 1\right)}{\left(\frac{P_t}{d_s}\right)\left(\frac{P_l}{d_s}\right)} = \frac{\frac{\pi}{4} + \left(\frac{w_s}{d_s} - 1\right)}{\frac{P_t}{d_s} + \frac{a}{d_s} + \frac{w_s}{d_s}} \qquad (7)$$

for $\frac{w_s}{d_s} \geq 1$, where w_s is the slot length, d_s is the slot width, p_l is the longitudinal pitch (the center-to-center distance between two adjacent transverse rows of slots measured in the flow direction), and p_t is the traverse pitch (the distance between centers of the slots in adjacent longitudinal rows measured perpendicularly to the direction of flow). It is functions of three dimensionless parameters: w_s/d_s, p_t/d_s and p_l/d_s For the case of $w_s/d_s = 1$, σ_s of the oval slotted pattern reduces to that of the round cicle pattern. $a/d_s = 0$ corresponds to the case of an infinite slot.

Both the round hole patterns and the oval slotted patterns with a= w_s each having five plate surface porosities of 5.7, 12.8, 17.4, 22.8, and 28.8%, were fabricated and tested. The surface porosity was changed by varying the center-to-center distance d or p_l.

Three plate spacings were tested: 0.974", 0.47" and 0.221." For the plate thickness of 1/32", the thickness-spacing ratios were 0.0321, 0.0665, and 0.141, respectively. The t/b ratios for a plate-fin heat exchanger with rectangular fins of 0.004-inch thickness are 0.046 and 0.0962 for the fin pitches of 11 and 22 fins per inch, respectively.

The test results were correlated for the j and f factors and their ratio against the plate surface porosity with the Reynolds number as parameter. Figs. 7, 8 and 9 depict those for t/b = 0.141, 0.0665, and 0.032, respectively for the round cicle perforation. The friction factor was also plotted against the Reynolds number in these figures, from which the Reynolds number for the transition of flow from laminar to turbulent patterns can be identified. Correction of f to account for the inlet and exit pressure losses were found to be negligible using a figure available in Reference [4]. The lowest possible Reynolds number

or air flow through the test core was dictated by the reading of the micromanometer (limited to 0.001 inch of water column).

It is seen in Figs. 7C, 8C and 8C that the variation of f/j values with the plate surface porosity σ_s for the round cicle perforation seems to follow a particular pattern: it takes a maximum value at σ_s of approximately 6% then decreases to a value lower than that of a solid plate at about σ_s of 12.5% This suggests that round cicle perforated fins should be designed at σ_s of 12.5% or above for optimum heat transfer and friction loss performance. Furthermore, a comparison of these three figures reveals that f/j falls from the average value (averaged over σ_s from 0 to 22.8%) of approximately 2 to about unity and then rises to say 1.5 as the t/b ratio increases from 0.0321 to 0.0665 to 0.141. This indicates the existence of an optimum performance, i.e. corresponding to the minimum value of f/j, at the value of t/b around 0.0665.

Test results for the oval slotted plates were shown in Figs. 10, 11 and 12. The general feature of the heat transfer and friction behavior resembles that of the round cicle perforated plates, as evidence in the average value of f/j, its variation with t/b and the delay of flow transition. An important difference between the two perforation geometries is that there is an indication of the minimum j/f at σ_s of 17.4% in the case of the slotted pattern. For the round circle pattern, the minimum j/f seems to be at σ_s of 12.5% (for t/b of 0.0321 and 0.0665) or high (for t/b - 0.141).

An important conclusion from the test results is the confirmation of geometric and dynamic similarities through the following two observations. First, the transition of air flow from laminar into turbulent patterns is delayed from Re = 2,000 to about 3,500 as t/b decreases from 0.2 to 0.0964, as illustrated in Fig. 13

(reproduced from Reference 2). The same phenomenon is observed in the present results. The transition is delayed from Re = 2,000 to 5,000, to 10,000 as t/b decreases from 0.141 to 0.0665, to 0.0321. Second, the values of f/j for the plate surface porosities of 12.5% and 25% in Reference 2 are practically the same. The equal value of f/j for the two porosities is confirmed in the present results for both perforated patterns.

COMPARISON OF TEST RESULTS WITH THEORY

The test results indicate the values of f/j vary between 0.5 to 2.5. The existing theory and experimental data for both the laminar and turbulent flows over the flat plate and inside ducts have confirmed the validity of these results: for laminar flows, it is well known that

$$f = \frac{4}{3Re_L^{1/3}} \quad , \qquad j = \frac{0.664}{Re_L^{1/2}}$$

$$f/j = 2.0 \tag{8}$$

for flow over a flat plate and

$$f = \frac{16}{Re_{D_h}} \quad , \qquad j = \frac{1.86}{(Re_{D_h})^{2/3}(L/D_h)^{1/3}}$$

$$f/j = 8.6\left(\frac{L/D_h}{Re_{D_h}}\right)^{1/3}, \quad \delta = \frac{5(X/D_h)}{Re_{D_h}^{1/2}} \tag{9}$$

for flow inside ducts. Here, the subscripts L and D_h refer to the characteristic length to be employed in the Reynolds number, δ is the thickness of boundary layer at location X. In case of turbulent flows, one knows that

$$f = \frac{0.072}{Re_L^{1/5}} \quad , \qquad j = \frac{0.036}{Re_L^{1/5}}$$

$$f/j = 2.0 \tag{10}$$

for flow over a flat plate and

$$f = 0.046\, Re_{D_h}^{-0.2} \quad , \qquad j = 0.023\, Re_{D_h}^{-0.2}$$

$$f/j = 2.0, \quad \delta = 0.376\, X \left(\frac{X}{D_h}\right)^{-1/5} Re_{D_h}^{-1/5} \tag{11}$$

for flow inside ducts.

For example, for a laminar flow through a rectangular duct of $\ell/D_h = 6$ (equivalent to the test core with the plate spacing of 1 inch) with Re_{Dh}=3,000, equation (9) gives f/j=1.08. The presence of perforated holes should not change substantially the order of magnitude of f/j. The actual flows through the test cores may take one or a combination of the above-mentioned four flow cases, depending mainly on the magnitude of the Reynolds number.

In comparison with high performance of the test cores as evidenced by low values of f/j, compact heat exchangers have substantially higher f/j values due to the following factors.

(i) Influence of brazing roughness [5].

(ii) Flow passage-to-passage dimensional variations which depend on manufacturing tolerance [6] and technique.

(iii) Aerodynamic cleanliness of the leading edges of the fin and plate surfaces at inlet [1] and the edges of the perforated holes.

(iv) Influence of fouling which depends on the details of heat exchanger service conditions.

Attempts have been made to develop equations for correlating the test results based on the existing theory and experimental data available for flows over a flat plate with an infinite slot normal to the flow direction. Hangen and Dhanak [7,8] have analytically and experimentally investigated the heat transfer and friction loss performance in the separate-flow region of a rectangular cavity facing an oncoming turbulent boundary layer. Both the f and j factors are correlated as functions of δ'/b for $0.5 \leqslant h'/b \leqslant 2$, where δ' is the thickness of boundary layer at the leading edge of the cavity and h' is the depth of the cavity. Their results were converted to the form suitable for the present study as

$$f_c = 0.022\left[1-\left(\frac{2P_l-d_s}{d_s}\right)\left(\frac{2P_l-d_s}{D_h}\right)^{-1/5}\left(Re_{D_h}\right)^{-1/5}\right] \tag{12}$$

$$j_c = 0.243\left(1+\frac{d_s}{t}\right)^{-1/2}\left(\frac{2P_l-d_s}{d_s}\right)^{0.11}\left(\frac{2P_l-d_s}{D_h}\right)^{-0.222} P_r^{2/3} Re_{D_h}^{-0.222} \tag{13}$$

where d_s must be replaced by d in the case of the round hole pattern, x is the distance measured from the leading edge of the cavity as illustrated in Fig. 6 and the subscript C refers to the case of an infinite cavity.

For calculating the heat trasnfer and friction loss performance, a perforated plate is considered consisting of three (or two) portions as shown in Fig. 6: (I) perforated portion, (II) nonperforated portion in between two adjacent holes in the flow direction, and (III) nonperforated portion along which flow does not meet holes. The last portion III exists only if $w_s \geqslant a$ for the slotted pattern and $\ell \geqslant 2d$ for the round hole pattern. Equations (4) for turbulent flow over a flat plate are used to evaluate j_{II} and F_{II} in portion II. Both laminar and turbulent patterns are employed for the flow over portion III. In the range of $0 \leqslant x \leqslant \delta$ equations (8) or (10) for flows over a flat plate are employed, while in the range of $x \geqslant \delta$, equations (9) or (11) for flows inside ducts are used. The overall heat transfer factor of the perforated plate is equal to the sum of the j factor-area fraction products of the individual portions:

$$j_T = j_I\sigma_I + j_{II}\sigma_{II} + j_{III}\sigma_{III} \tag{14}$$

where $\sigma_I = \sigma_s, j_I = j_c$ and σ_{II} and σ_{III} are the area fractions of portions II and III, respectively. $\sigma_{III} = 0$ when $a \geqslant w_s$ or $d \geqslant \ell/2$. Similarly, the overall friction factor of the perforated plate is

$$f_T = f_I\sigma_I + f_{II}\sigma_{II} + f_{III}\sigma_{III} \tag{15}$$

where $F_I = f_c$. Both the $j_{III}\ \sigma_{III}$ and $f_{III}\ \sigma_{III}$ terms consist of two parts: one is contributed by flow over a flat plate in $0 \leqslant x \lesssim \delta$ and the other is contributed by flow inside ducts in $x \gtrsim \delta$. Using the test data as inputs, j_T and f_T were calculated by means of a digital computer. The results were plotted in Figs. 7,8,9, and 10 for comparison with the experimental results. Solid lines indicate that the turbulent flow equations (8) and (9) were employed for the evaluation of j_{III} and f_{III}. Broken lines refer to the use of laminar-flow equations (10) and (11) for evaluating j_{III} and f_{III}. It is seen in the figures that equations (14) and (15) predict the monotonic variations of j_T and f_T with σ_s. At least, these equations predict accurate orders of magnitude for both j_T and f_T in spite of the use of the empirical results for an infinite rectangular cavity. This gives us additional confidence in the test results.

CONCLUSION

A large scale technique is developed to examine the effects of perforation geometry on the heat transfer and friction loss performance of compact heat exchangers of the plate-perforated rectangular fin surfaces. Through the comparison of the test results with those of the compact heat exchangers of different scale, the geometric and dynamic similarities of both systems are confirmed. In other words, the validity of the large scale technique is thus established. The technique is simple and quick to carry out and may also be employed to determine the optimum perforation geometry and to understand or interpret test data from a compact heat exchanger. It is shown that the heat transfer to friction factor ratio for a perforated plate of very low surface porosity is higher than that of a solid plate. This means, a plate-fin heat exchanger of plain fin geometry will have more attractive heat transfer and friction performance than the same type heat exchanger with perforated fins of low porosity.

The following conclusions are obtained from the present study.

(1). The slotted pattern seems to give more attractive f/j values than the round hole pattern.

(2). The optimum surface porosities for both the round hole and slotted patterns seem to be between 12 and 20 percent.

(3). The optimum t/b ratio is between 0.0665 and 0.141 for both perforation patterns.

More parametric studies of the plates with slotted perforation are needed for more definite conclusions.

REFERENCES

1. W.M. Kays and A.L. London, Compact Heat Exchangers, 2nd Ed., McGraw-Hill Book Co., New York (1964).

2. S. Wong, J.D. Duncan, D.W. Graumann, J.C. Gibson, and J.J. Killackey, "Compact Condenser for Rankine Cycle Engine", Final Report 71-7464 (prepared for Office of Air Programs, Environmental Protection Agency, Ann Arbor, Michigan) AiResearch Manufacturing Co., Los Angeles, Calif. (June 1971).

3. J.A. Clark, C.A. Siebert, R.B. Keller, M. Borden, and J.C. Hoo, "Automotive Radiators Manufactured by the Electroforming Process", Final Report of ORA Project 05335 (under contract with International Copper Research Association, Inc., New York), University of Michigan, Ann Arbor, Michigan (December 1964).

4. W.H. McAdam, Heat Transmission, 2nd Ed., McGraw-Hill Book Co., New York (1955).

5. R.K. Shah and A.L. London, "Influence of Brazing on Very Compact Heat Exchanger Surfaces", ASME Paper No. 71-HT-29 presented at the ASME-AIChE Heat Transfer Conference, Tulsa, Okla. (Aug. 1971).

6. A.L. London, "Laminar Flow Gas Turbine Regenerators - the Influence of Manufacturing Tolerances", Trans. ASME, Journal of Engineering for Power, 92, Ser. A, pp. 46-56 (1970).

7. R.L. Hangen and A.M. Dhanak, "Momentum Transfer in Turbulent Separated Flow Past a Rectangular Cavity", Journal of Applied Mechanics, Trans. ASME, Ser. A, 88, pp. 641-646 (1966).

8. R.L. Hangen and A.M. Dhanak, "Heat Transfer in Turbulent Boundary-Layer Separation over a Surface Cavity", Journal of Heat Transfer, Trans. ASME, Ser. C, 89, pp. 335-340 (1967).

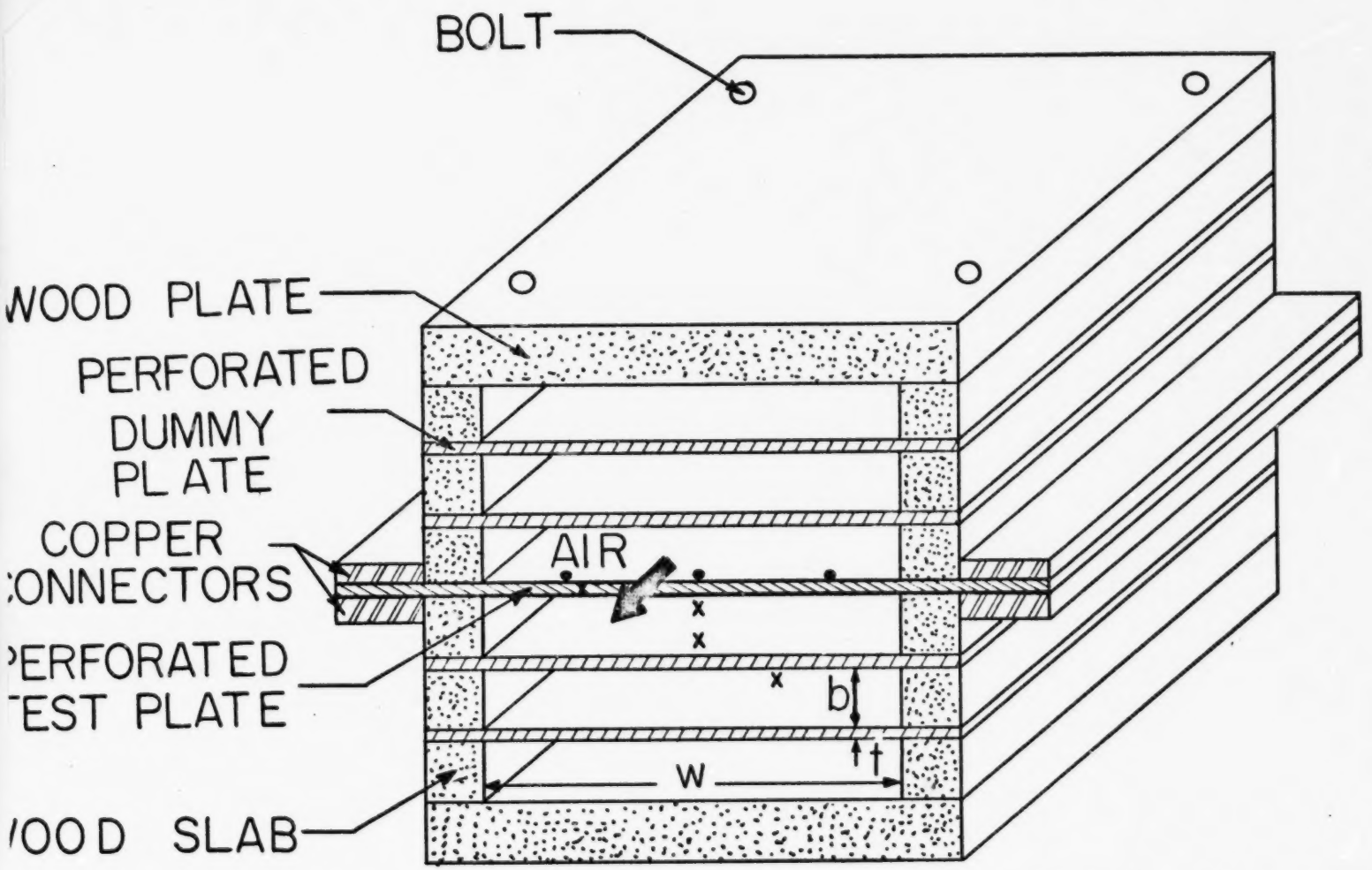

Fig.1 Heat exchanger test core and position (not exact location) of thermocouples

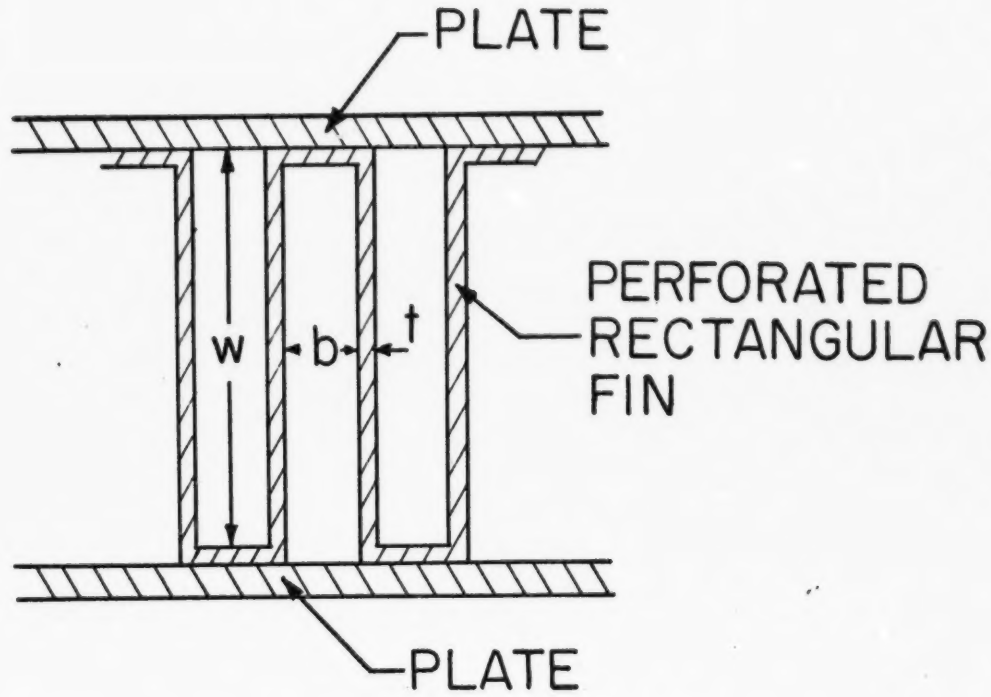

Fig.2 Plate-rectangular perforated fin surface

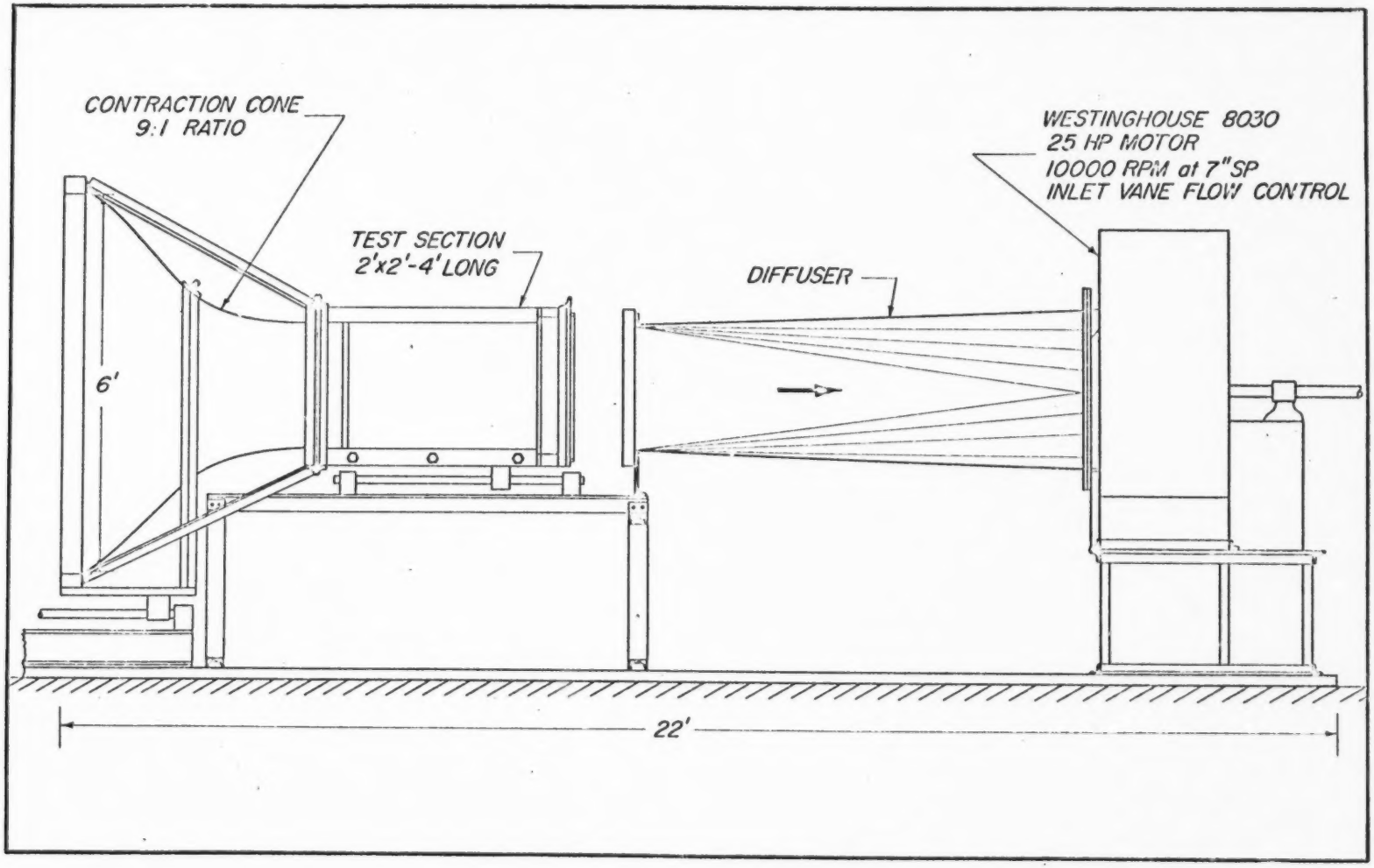

Fig.3 Wind tunnel

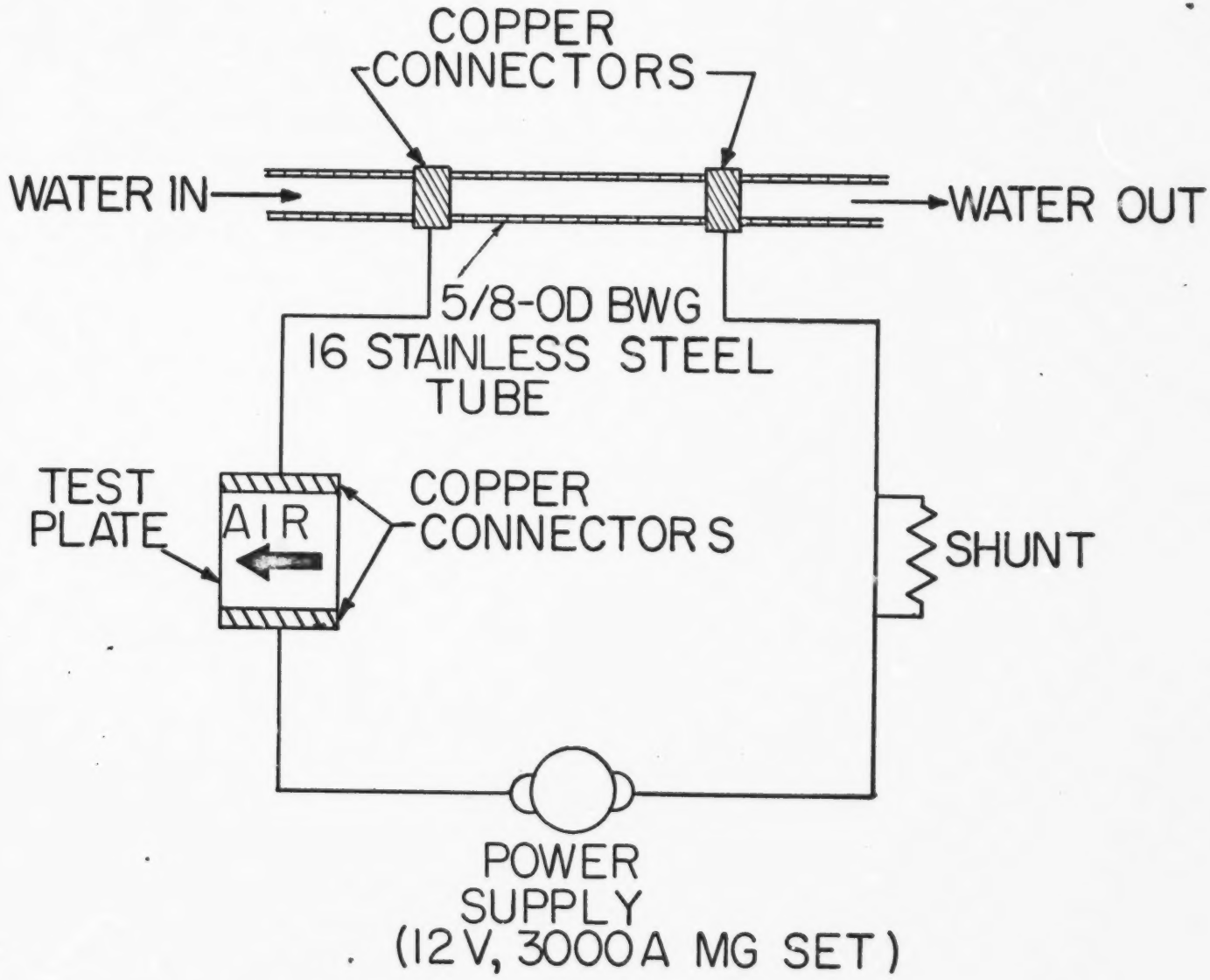

Fig.4 Schematic of electric power supply loop

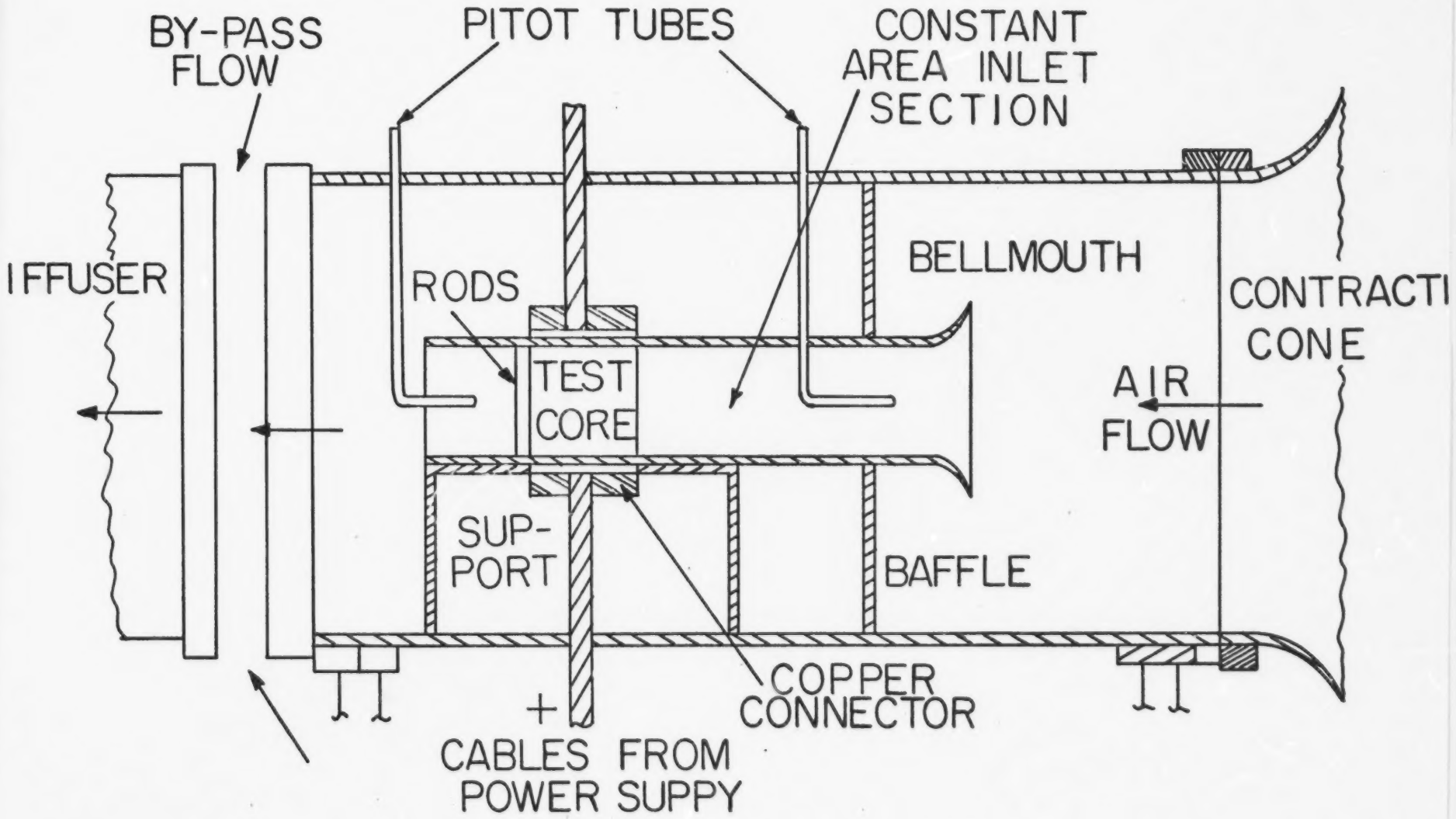

Fig.5 Schematic of test core installation in wind tunnel (elevation view)

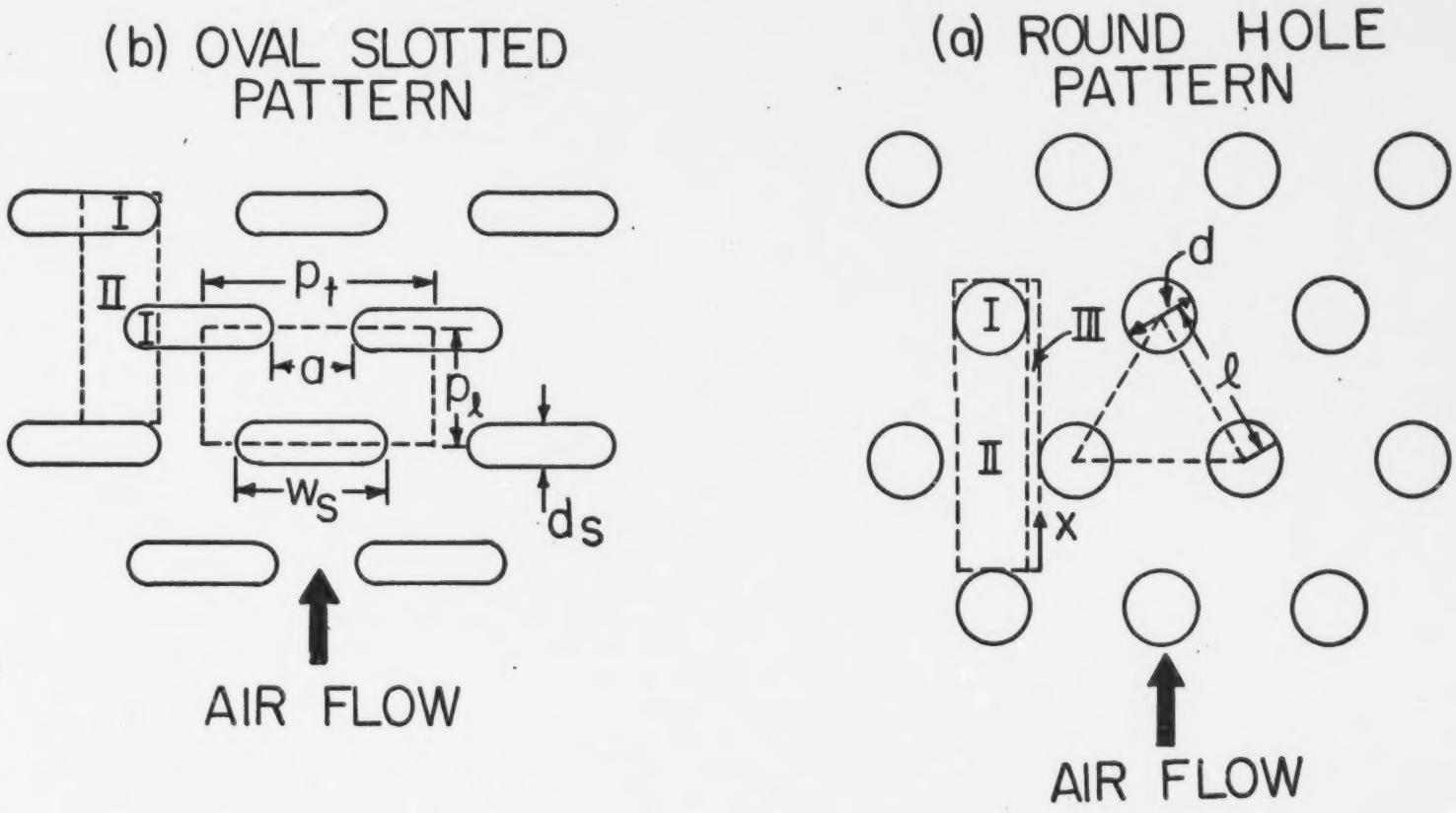

Fig.6 Perforation geometry

COMPUTER PROGRAM FOR DATA CORRELATION OF HEAT TRANSFER AND FRICTION LOSS OF PERFORATED PLATES IN WIND TUNNEL

```
      DIMENSION TA(4), AREA(4)
C READ INPUT DATA
      READ(5,1)EPSI, GAP, N
    1 FORMAT(2F10.1, I2)
      WRITE(6, 2)EPSI, GAP
    2 FORMAT ('1 SPEC.:    POROSITY = ', F6.4, 3X, 'GAP = ', F6.4)
C
      DO 30 I = 1, N
      READ(5,5)TP1, TP2, TP3, TA(1), TA(2), TA(3), TA(4), TIN
    5 FORMAT(8F10.1)
      READ(5, 10)P11, PVOLT, SVOLT, V
   10 FORMAT(4F10.1)
C CAL REYNOLD NO
      R = GAP/(4.*(6.+ GAP))
      AETA = 60.*.00017
      RE = 4.*R*V/AETA
C  TEMP AND POWER
      TP = (TP1 + TP2 + TP3)/3.
      POWER = PVOLT*SVOLT*341200.
      STEP = GAP/3.
      CALL QSF(STEP, TA, AREA, 4)
      TOUT = AREA(4)/GAP
      TBULK = .5*(TIN + TOUT)
      DELT = TP - TBULK
C PERFORMANCE CALCULATION
      H = 2.*POWER/DELT
      HJ = .761*H/V
      F=32500000.*P11*R/(V*V)
      FJ = F/HJ
C RESULTS
      WRITE(6,26)TP1, TP2, TP3, TA(1), TA(2), TA(3), TA(4), TIN
   26 FORMAT('0 INPUT:', 2X, 8F8.2)
      WRITE(6,27)P11,PVOLT,SVOLT,V
   27 FORMAT(' ', 10X, 3F10.4, F10.1)
      WRITE(6, 28)V, RE, TP,TOUT, DELT
   28 FORMAT(' OUPUT:',2X,'VEL=',F6.1,4X,'RE=',F8.1,4X,'PL T=',F6.2,4X,
     1   'TE=',F5.1,3X,'DELT=', F5.1)
      WRITE(6, 29)POWER, H, HJ, F, FJ
   29 FORMAT(' ', 8X,'Q=',F6.1,3X,'H=',F7.3,3X,'J=',F8.6,3X,'F=',F7.5,
     1   3X, 'F/J=',F6.4)
   30 CONTINUE
      END
```

COMPUTER PROGRAM FOR HEAT TRANSFER AND FRICTION LOSS PERFORMANCE OF ROUND HOLE PLATES -- TURBULENT FLOW MODEL FOR REGION III

```
C       CIRCULAR CAVITIES
        DIMENSION S(4)
        READ (5,1001) T,S1,TL,S3,D,PR
        WRITE(6,1001) T,S1,TL,S3,D,PR
 1001 FORMAT (2F10.5,4F10.3)
        DH=2.0*S1*S3/(S1+S3)
        DS=DH/S1
        DT=TL/DH
        DD=D/DH
        DT=D/T
C       DL=L/DH, DS=DH/S, DD=D /DH, DT=D*/T
        D1=DT**0.2
        D2=DD**0.2
        D3=DD**0.222
        D4=DT**0.5
        D5=DT**0.334
        READ (5,1002) (S(J),J=1,4)
 1002 FORMAT (4F10.3)
    1 READ (5,1111,END=100) RE
 1111 FORMAT (F10.1)
        WRITE(6,1003) RE
 1003 FORMAT(//'RE=',F7.1)
        R1=RE**0.2
        R2=RE**0.222
        R3=RE**0.5
        R4=RE**0.667
        WRITE (6,1004)
 1004 FORMAT (//3X,'SIGMA',6X,'CF',9X,'F',9X,'J',7X,'CF/J',7X,'F/J'//)
C       FLOW OVER PLATE ZONE, TURBULENT
        X=(0.5*S1*(RE/DH)**0.2/0.376)**1.25
        SS=0.
        WRITE (6,1101) X
 1101 FORMAT (//' X',F10.5//)
        DO 10 J=1,4
        SQ=SQRT(S(J))
        CF=0.022*(S(J)-SQ*(0.9514-SQ)/((1.0-1.051*SQ)**0.2*D2*R1))
       1+0.074*(2.1*SQ-S(J))/((1.0-1.051*SQ)**0.2*D2*R1)
        CJ=0.365/(0.376**0.14)*S(J)**0.445*(0.9514-SQ)**0.11*PR**0.667*
       1(0.3*SQ+0.28/DT)/((1.0-1.051*SQ)**0.222*D3*R2)
       2+0.036*(2.1*SQ-S(J))/((1.0-1.051*SQ)**0.2*D2*R1)
C       TURBULENT PLATE CF1,CJ1.  TURBULENT DUCT CF2,CJ2
        CF1=0.074/(D2*R1)*(1.0-2.1*SQ)
        CJ1=0.036/(D2*R1)*(1.0-2.1*SQ)
        CF2=0.184/R1*(1.0-2.1*SQ)/4.0
        CJ2=0.023/R1*(1.0-2.1*SQ)
        IF (X.GE.TL) GO TO 5
        F=(CF+CF1*X/TL)*0.5*DS+(1.0-X/TL)*CF2
        CF=CF+CF1*X/TL+(1.0-X/TL)*CF2
        CJ=CJ+CJ1*X/TL+(1.0-X/TL)*CJ2
        GO TO 6
    5 F=(CF+CF1)*0.5*DS
        CF=CF+CF1
        CJ=CJ+CJ1
    6 FJ=CF/CJ
        FEJ=F/CJ
```

```
      WRITE(6,1005) S(J),CF,F,CJ,FJ,FBJ
 1005 FORMAT (6F10.5)
   10 CONTINUE
      WRITE(6,1004)
      DO 15 K=1,12
      SQ=SQRT(SS)
      CF=0.022*(SS  -SQ*(0.9514-SQ)/((1.0-1.051*SQ)**0.2*D2*R1))
     1+0.074*(2.1*SQ-SS  )/((1.0-1.051*SQ)**0.2*D2*R1)
      CJ=0.365/(0.376**0.14)*SS  **0.445*(0.9514-SQ)**0.11*PR**0.667*
     1(0.3*SQ+0.28/DT)/((1.0-1.051*SQ)**0.222*D3*R2)
     2+0.036*(2.1*SQ-SS  )/((1.0-1.051*SQ)**0.2*D2*R1)
      CF1=0.074/(D2*R1)*(1.0-2.1*SQ)
      CJ1=0.036/(D2*R1)*(1.0-2.1*SQ)
      CF2=0.184/R1*(1.0-2.1*SQ)/4.0
      CJ2=0.023/R1*(1.0-2.1*SQ)
      IF (X.GE.TL) GO TO 11
      F=(CF+CF1*X/TL)*0.5*DS+(1.0-X/TL)*CF2
      CF=CF+CF1*X/TL+(1.0-X/TL)*CF2
      CJ=CJ+CJ1*X/TL+(1.0-X/TL)*CJ2
      GO TO 12
   11 F=(CF+CF1)*0.5*DS
      CF=CF+CF1
      CJ=CJ+CJ1
   12 FJ=CF/CJ
      FBJ=F/CJ
      WRITE(6,1005) SS  ,CF,F,CJ,FJ,FBJ
      SS=SS+0.02
   15 CONTINUE
      GO TO 1
  100 CONTINUE
      CALL EXIT
      END
```

COMPUTER PROGRAM FOR HEAT TRANSFER AND FRICTION LOSS PERFORMANCE OF ROUND HOLE PLATES -- LAMINAR FLOW MODEL FOR REGION III

```
C       CIRCULAR CAVITIES
        DIMENSION S(4)
        READ (5,1001) T,S1,TL,S3,D,PR
        WRITE(6,1001) T,S1,TL,S3,D,PR
 1001 FORMAT (2F10.5,4F10.3)
        DH=2.0*S1*S3/(S1+S3)
        DS=DH/S1
        DL=TL/DH
        DD=D/DH
        DT=D/T
C       DL=L/DH, DS=DH/S, DD=D*/DH, DT=D*/T
        D1=DL**0.2
        D2=DD**0.2
        D3=DD**0.222
        D4=DL**0.5
        D5=DL**0.334
        READ (5,1002) (S(J),J=1,4)
 1002 FORMAT (4F10.3)
    1 READ (5,1111,END=100) RE
 1111 FORMAT (F10.1)
        WRITE(6,1003) RE
 1003 FORMAT(//'RE=',F7.1)
        R1=RE**0.2
        R2=RE**0.222
        R3=RE**0.5
        R4=RE**0.667
        WRITE (6,1004)
 1004 FORMAT (//3X,'SIGMA',6X,'CF',9X,'F',9X,'J',7X,'CF/J',7X,'F/J'//)
C       FLOW OVER PLATE ZONE, LAMINAR
        X=0.01*RE*S1/DS
        SS=0.
        WRITE (6,1101) X
 1101 FORMAT (//' X',F10.5//)
        DO 10 J=1,4
        SQ=SQRT(S(J))
        CF=0.022*(S(J)-SQ*(0.9514-SQ)/((1.0-1.051*SQ)**0.2*D2*R1))
       1+0.074*(2.1*SQ-S(J))/((1.0-1.051*SQ)**0.2*D2*R1)
        CJ=0.365/(0.376**0.14)*S(J)**0.445*(0.9514-SQ)**0.11*PR**0.667*
       1(0.3*SQ+0.28/DT)/((1.0-1.051*SQ)**0.222*D3*R2)
       2+0.036*(2.1*SQ-S(J))/((1.0-1.051*SQ)**0.2*D2*R1)
C       LAMINAR PLATE CF1,CJ1.   LAMINAR DUCT CF2,CJ2
        CF1=1.33*(1.0-2.1*SQ)/(D4*R3)
        CJ1=0.664*(1.0-2.1*SQ)/(D4*R3)
        CF2=16.0*(1.0-2.1*SQ)/RE
        CJ2=1.86*(1.0-2.1*SQ)/(D5*R4)
        IF (X.GE.TL) GO TO 5
        F=(CF+CF1*X/TL)*0.5*DS+(1.0-X/TL)*CF2
        CF=CF+CF1*X/TL+(1.0-X/TL)*CF2
        CJ=CJ+CJ1*X/TL+(1.0-X/TL)*CJ2
        GO TO 6
    5 F=(CF+CF1)*0.5*DS
        CF=CF+CF1
        CJ=CJ+CJ1
    6 FJ=CF/CJ
        FBJ=F/CJ
```

```
      WRITE(6,1005) S(J),CF,F,CJ,FJ,FBJ
 1005 FORMAT (6F10.5)
   10 CONTINUE
      WRITE(6,1004)
      DO 15 K=1,12
      SQ=SQRT(SS)
      CF=0.022*(SS  -SQ*(0.9514-SQ)/((1.0-1.051*SQ)**0.2*D2*R1))
     1+0.074*(2.1*SQ-SS  )/((1.0-1.051*SQ)**0.2*D2*R1)
      CJ=0.365/(0.376**0.14)*SS  **0.445*(0.9514-SQ)**0.11*PR**0.667*
     1(0.3*SQ+0.28/DT)/((1.0-1.051*SQ)**0.222*D3*R2)
     2+0.036*(2.1*SQ-SS  )/((1.0-1.051*SQ)**0.2*D2*R1)
      CF1=1.33*(1.0-2.1*SQ)/(D4*R3)
      CJ1=0.664*(1.0-2.1*SQ)/(D4*R3)
      CF2=16.0*(1.0-2.1*SQ)/RE
      CJ2=1.86*(1.0-2.1*SQ)/(D5*R4)
      IF (X.GE.TL) GO TO 11
      F=(CF+CF1*X/TL)*0.5*DS+(1.0-X/TL)*CF2
      CF=CF+CF1*X/TL+(1.0-X/TL)*CF2
      CJ=CJ+CJ1*X/TL+(1.0-X/TL)*CJ2
      GO TO 12
   11 F=(CF+CF1)*0.5*DS
      CF=CF+CF1
      CJ=CJ+CJ1
   12 FJ=CF/CJ
      FBJ=F/CJ
      WRITE(6,1005) SS  ,CF,F,CJ,FJ,FBJ
      SS=SS+0.02
   15 CONTINUE
      GO TO 1
  100 CONTINUE
      CALL EXIT
      END
```

```
C       ****SLOTS****
        READ (5,1001) B,C,T,S,W,TL,PR
        WRITE(6,1001) B,C,T,S,W,TL,PR
 1001 FORMAT (6F10.5,F10.2)
        DH=2.0*S*W/(S+W)
        DS=DH/S
        B1=(S/DH)**0.2
        B2=(B/DH)**0.222
        A=(4.0*C+3.1416*B)/(4.0*(B+C))
        G=0.365/(0.376**0.14)
    1 READ (5,1002,END=100) RE
 1002 FORMAT (F10.2)
        WRITE(6,1003) RE
 1003 FORMAT (//'RE=',F7.2/)
        XC=(0.5*S*(RE/DH)**0.2/0.376)**1.25
        R1=RE**0.2
        R2=RE**0.222
        R3=(0.5*S/B)**0.14*(B*RE/DH)**0.25
        XD=(XC/DH)**0.2
        SMIN=(4.0*B*C+3.1416*B*B)/(4.0*TL*(B+C))
        WRITE(6,1006) SMIN
 1006 FORMAT (//'*** SMIN=',F7.5///)
        WRITE(6,1004)
 1004 FORMAT (//3X,'SIGMA',6X,'CF',9X,'F',9X,'J',7X,'CF/J',7X,'F/J'//)
        BR1=B1*R1
        CJG=G*PR**0.667*(0.3+0.294*T/B)
        BR2=B2*R2
        SS=0.
        CF1=0.074*(DH/XC)**0.2/R1*(XC/TL)
        CF2=0.046/R1*(1.0-XC/TL)
        CF=CF1+CF2
        F=0.5*DS*CF1+CF2
        CJ=0.036*(DH/XC)**0.2/R1*(XC/TL)+0.023/R1*(1.0-XC/TL)
        GO TO 20
    3 CONTINUE
        IF (SS.LT.SMIN) GO TO 30
        D=B*((4.0*C+3.1416*B)/(SS*(B+C)*4.0)-1.0)
        IF (D.LT.XC) GO TO 10
        CF1=(0.022-0.03*S/B)
        CF2=0.074/(XD*R1)*(XC/D)
        CF3=0.046/R1*(1.0-XC/D)
        CJ1=0.365*(0.3+0.294*T/B)/R3*PR**0.667
        CJ2=XC/D*0.036/(XD*R1)
        CJ3=(1.0-XC/D)*0.023/R1
        CF=CF1*SS+(1.0-SS)*(CF2+CF3)
        F=0.5*DS*(CF1*SS+(1.0-SS)*CF2)+CF3*(1.0-SS)
        CJ=CJ1*SS+(1.0-SS)*(CJ2+CJ3)
        GO TO 20
   10 CONTINUE
        FN=(A-SS)**0.2*BR1
        CF=0.022*(SS-SS**0.2*(A-SS)**0.8/BR1)+0.074*(1.0-SS)*SS**0.2/FN
        CJ=CJG*SS**1.112/((A-SS)**0.112*BR2)+0.036*(1.0-SS)*SS**0.2/FN
        F=0.5*DS*CF
   20 FJ=CF/CJ
        FBJ=F/CJ
```

```
      WRITE(6,1005) SS,CF,F,CJ,FJ,FBJ
 1005 FORMAT (6F10.5)
   30 CONTINUE
      SS=SS+0.01
      IF (SS.LE.A) GO TO 3
      GO TO 1
  100 CONTINUE
      CALL EXIT
      END
```

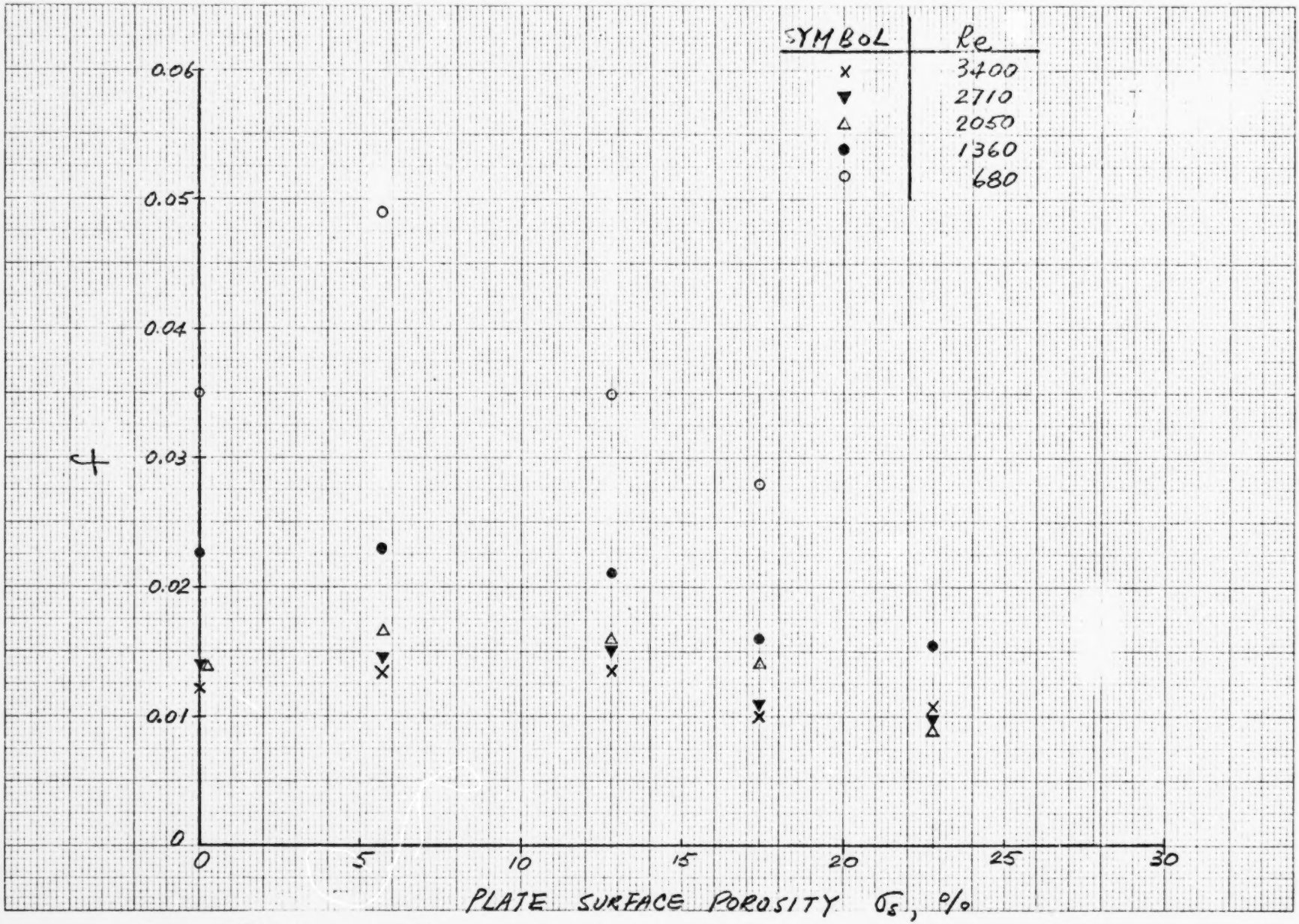

Fig 7a f vs σ_s for $t/b = 0.141$, round-circle patterns

Squares to the Inch

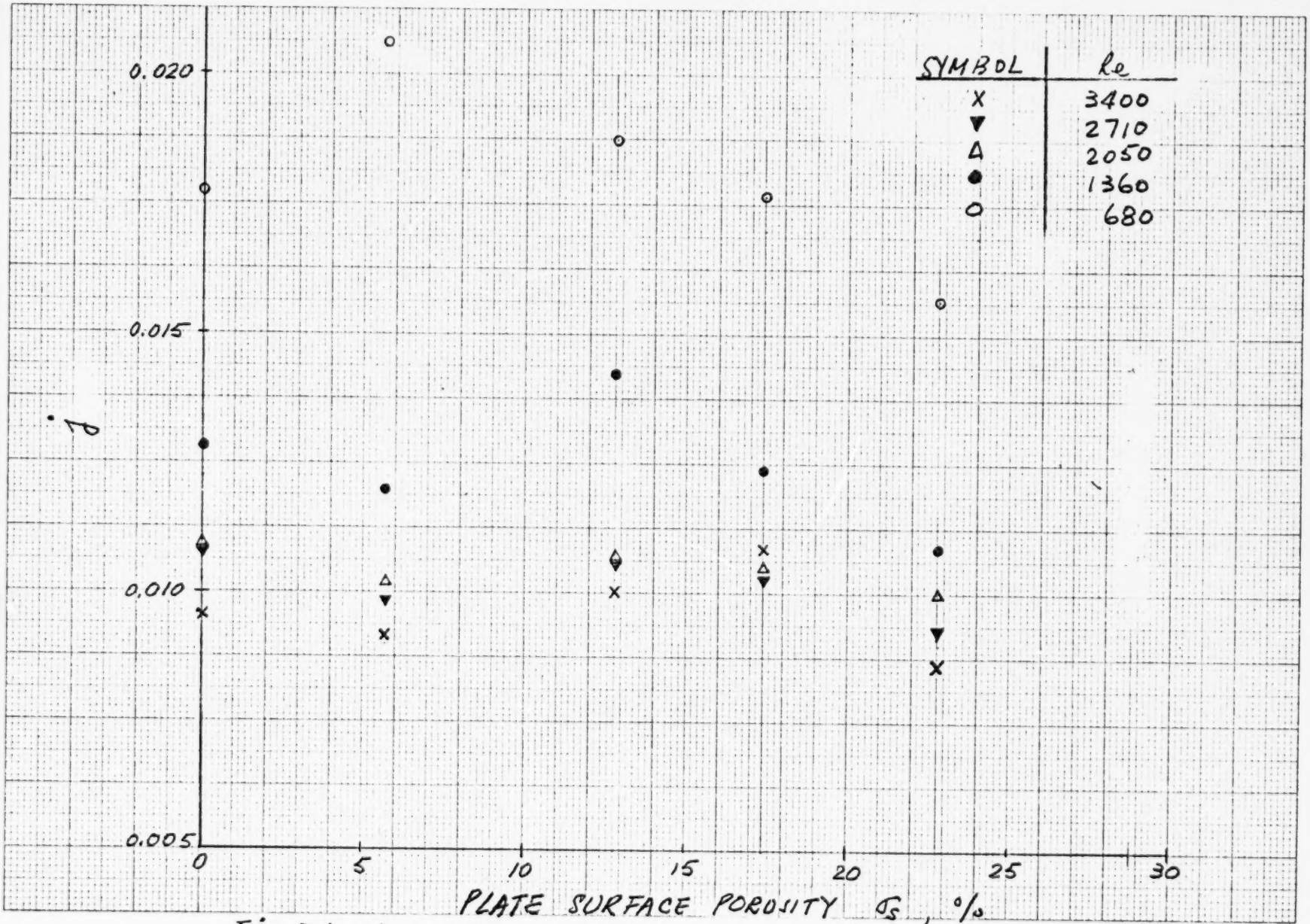

Fig 7b j vs σs for t/b = 0.141, round-circle pattern

Squares to the inch

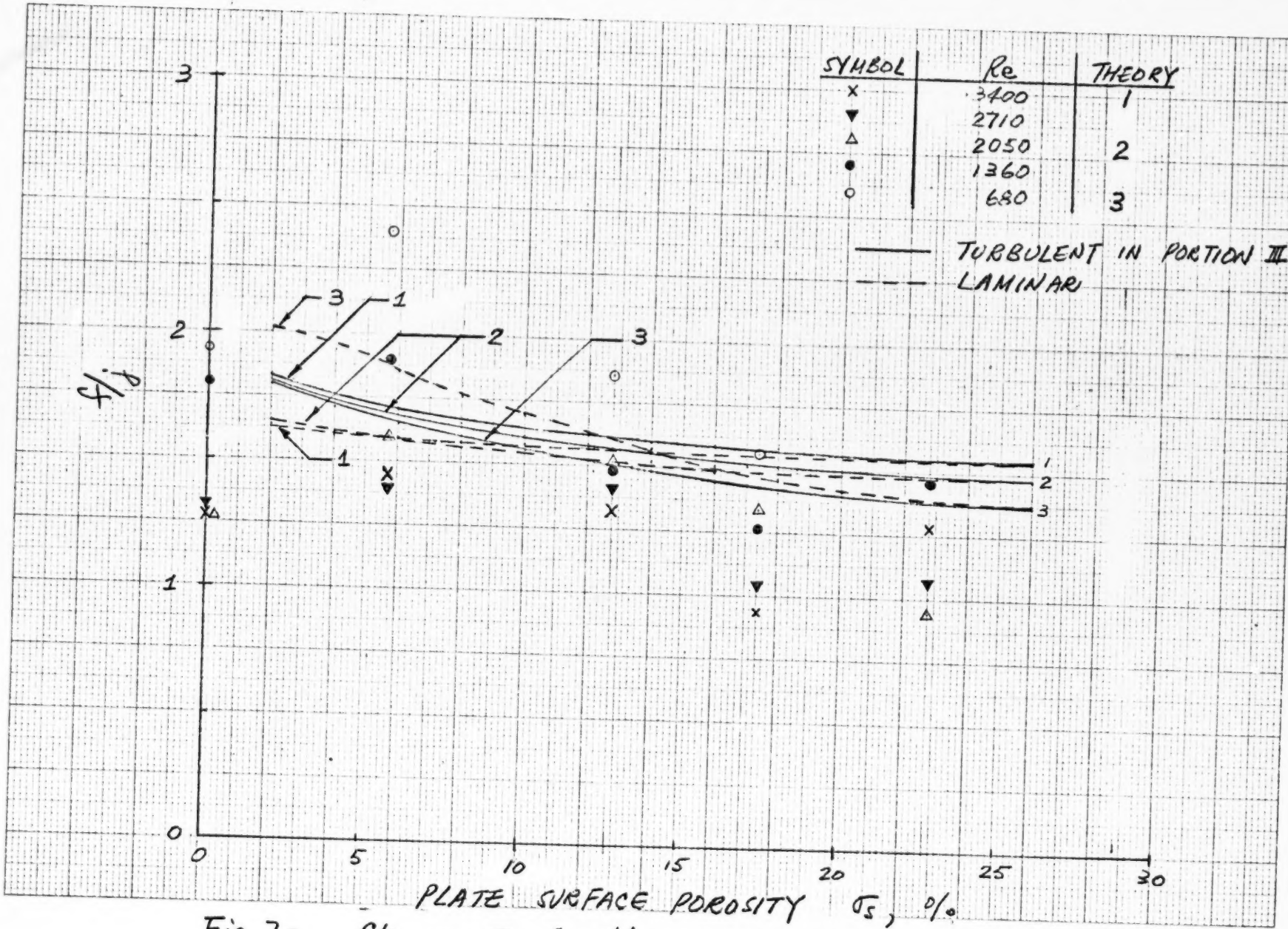

Fig 7c f/j vs σs for t/b = 0.141, round-circle patterns

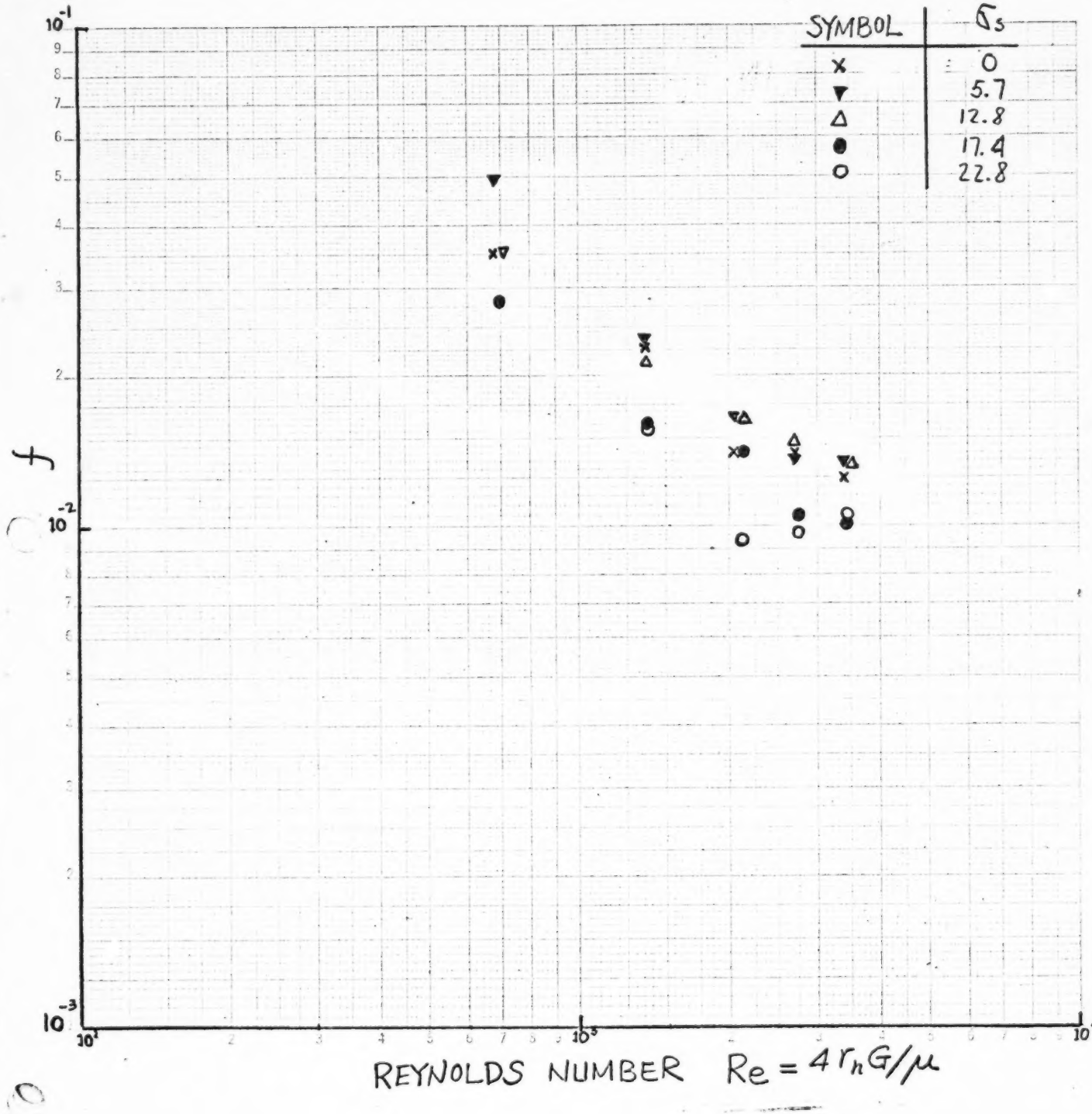

Fig. 7d f vs Re for $t/b = 0.141$, round-circle patterns

Logarithmic, 2 x 2 Cycles

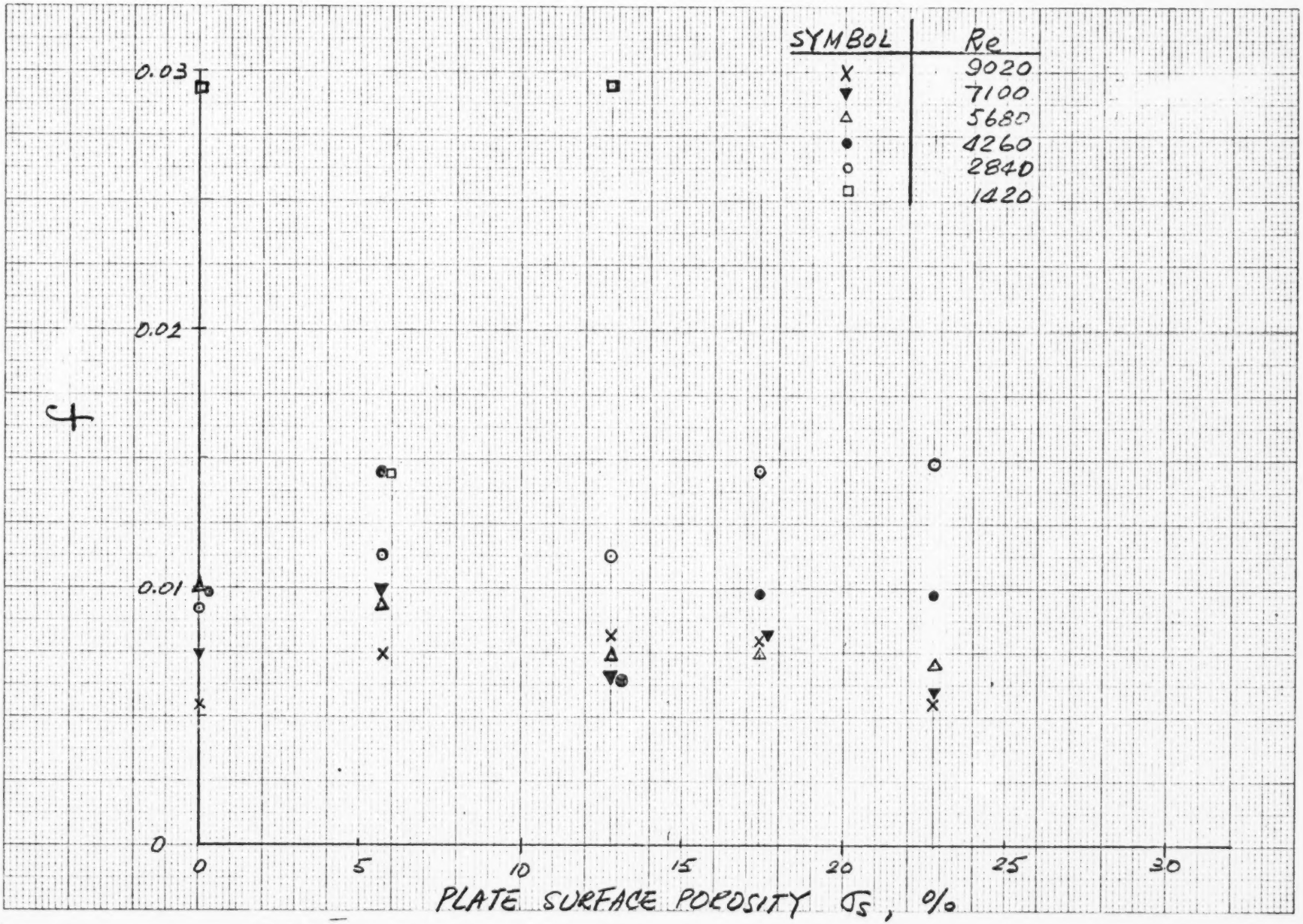

Fig 8a f vs σ_s for t/b = 0.0665, round circle patterns

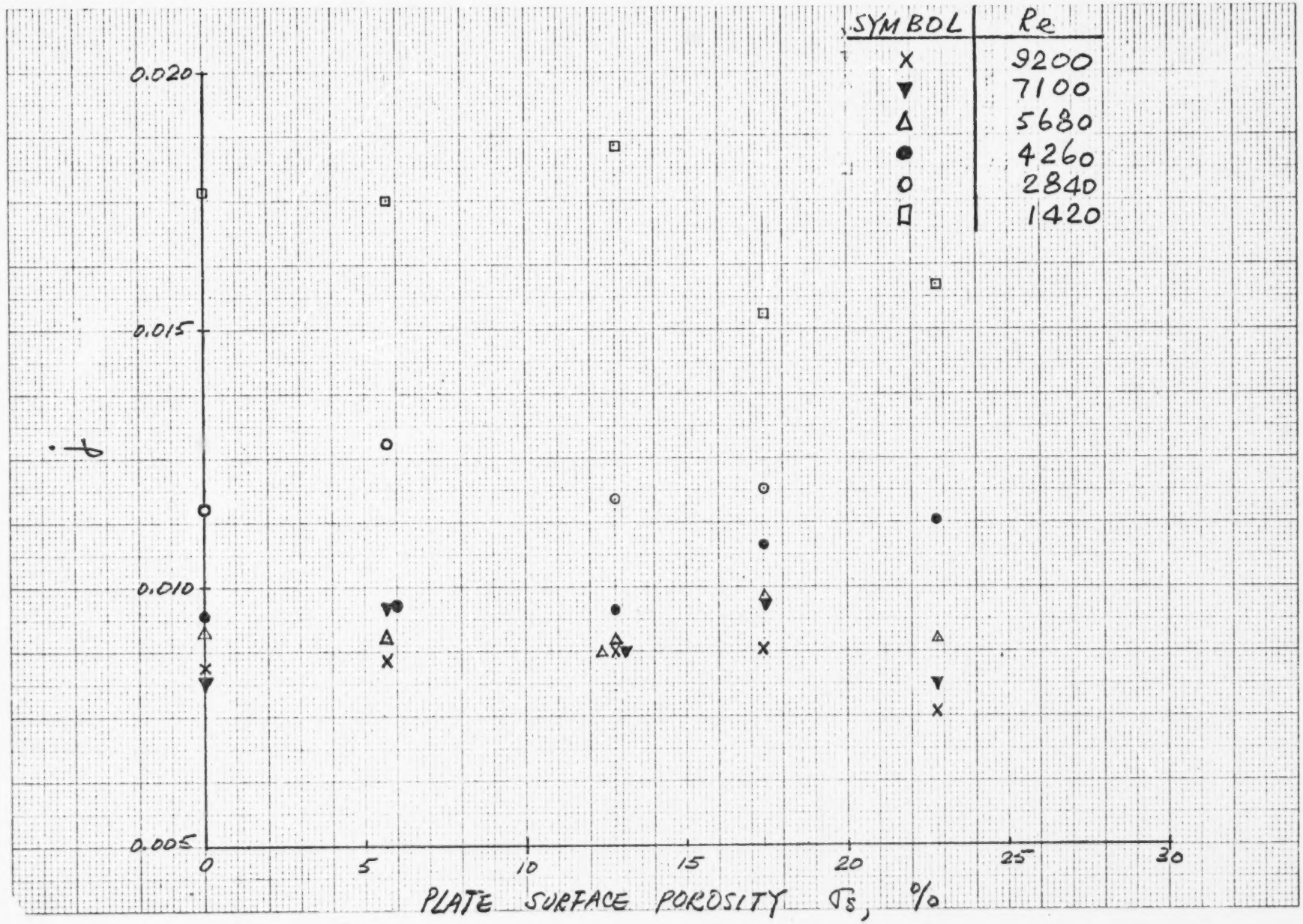

Fig 8b j vs σ_s for $t/b = 0.0665$, round-circle patterns

Squares to the inch

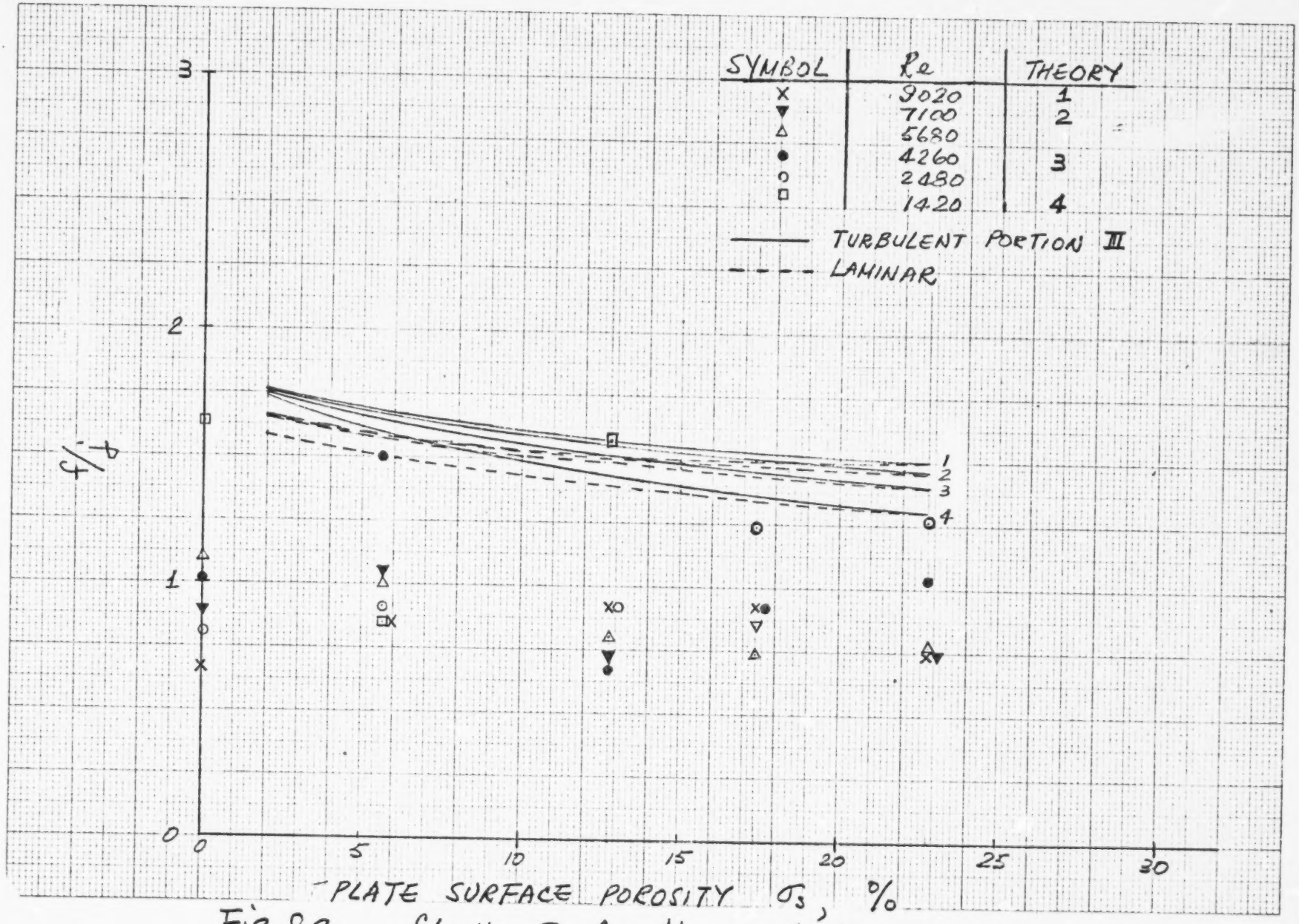

Fig 8C f/f_j vs σ_s for $t/b = 0.0665$, round circle patterns

Squares to the Inch

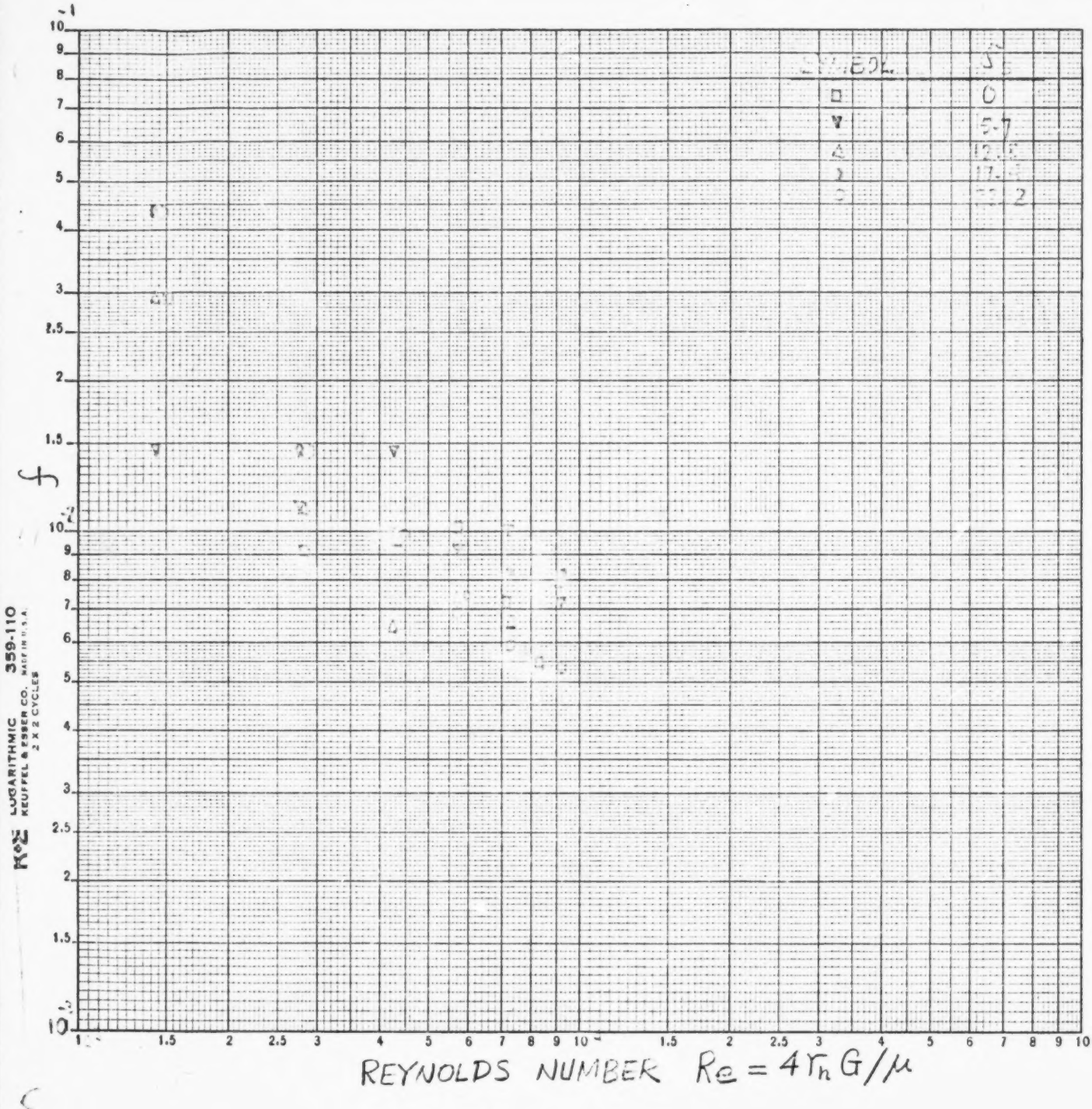

Fig. 8d f vs Re for $t/b = 0.0665$, round-circle patterns

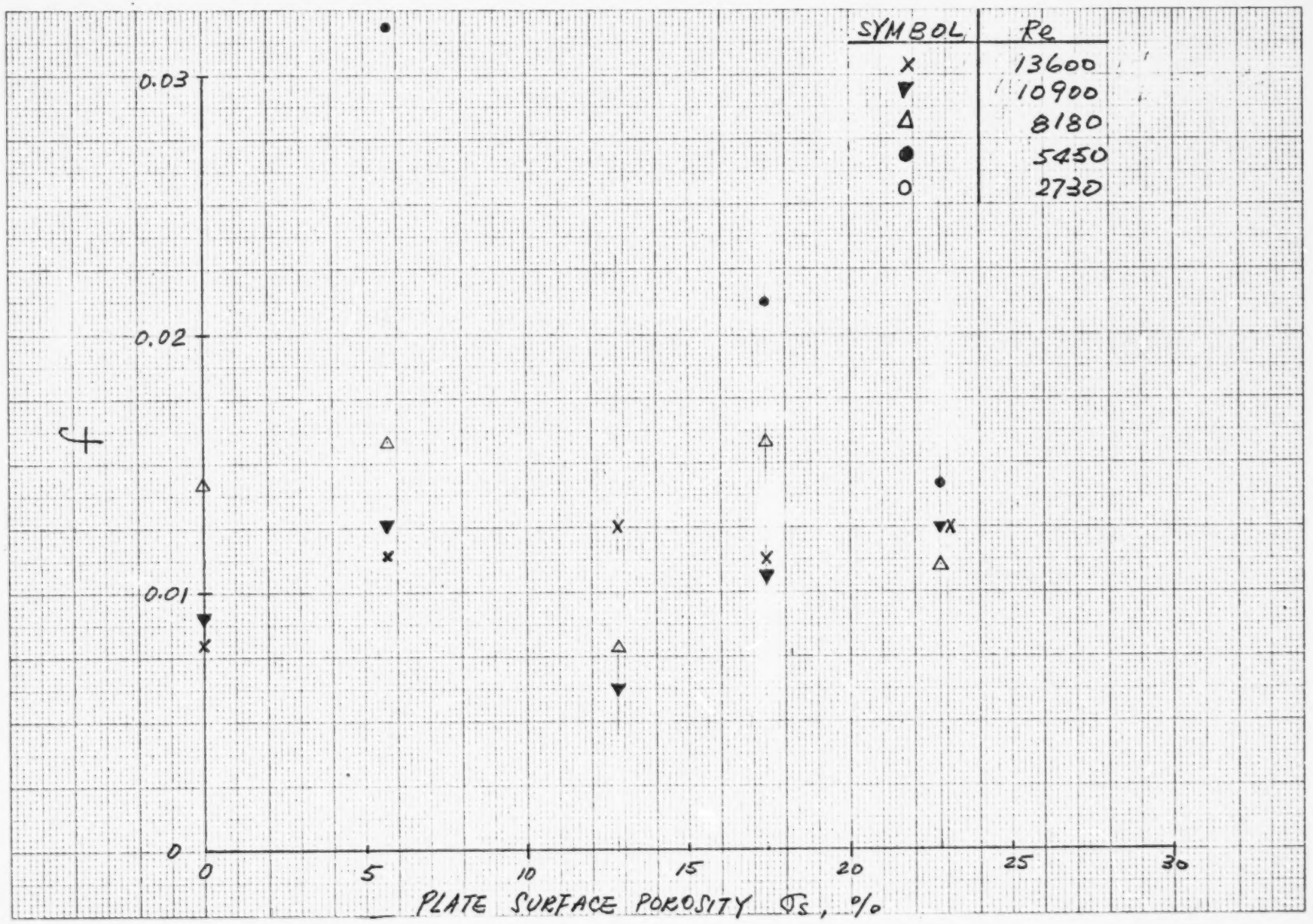

Fig 9a f vs σ_s for $t/b = 0.0321$, round-circle patterns

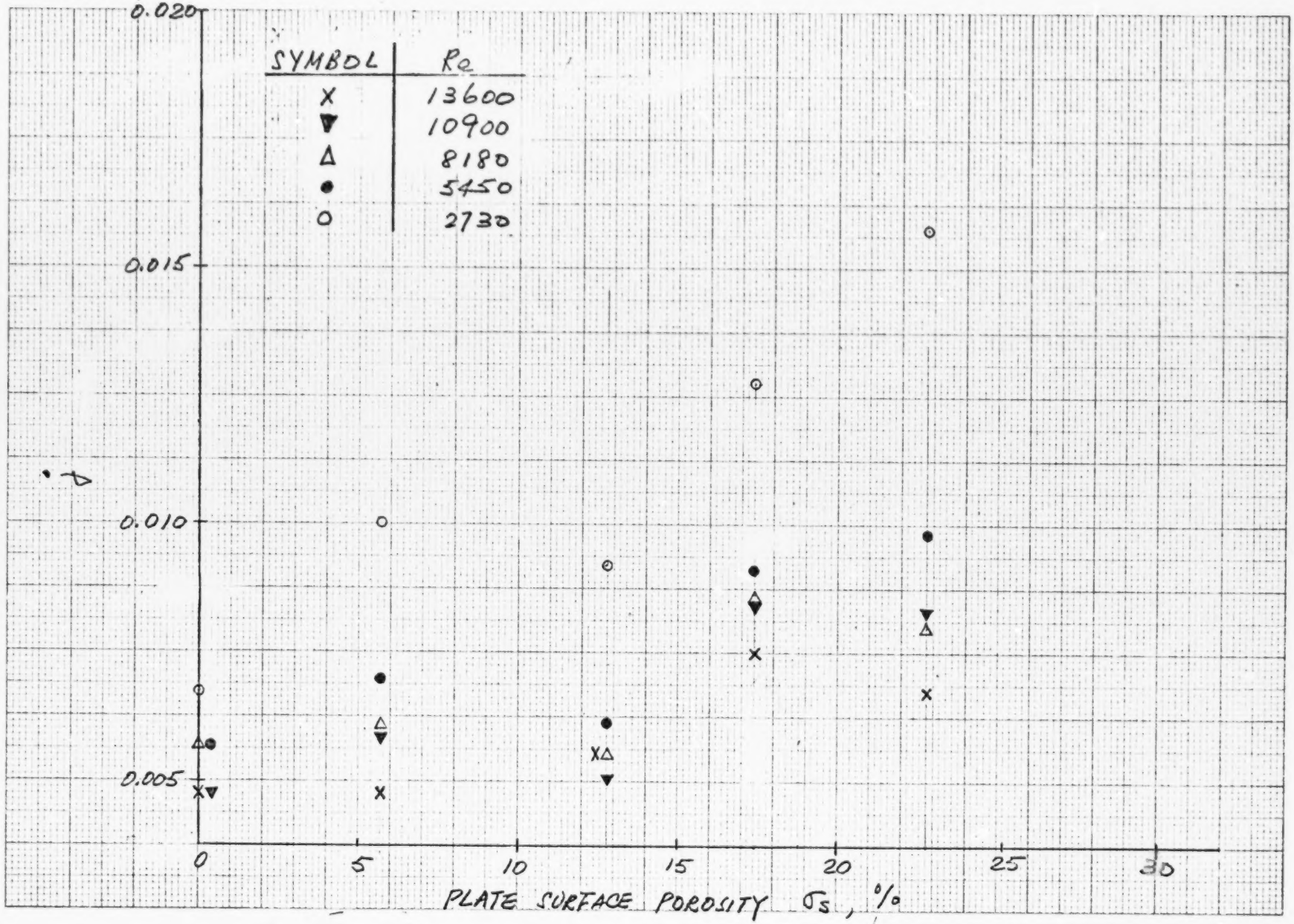

Fig 96 j vs σ_s for t/b = .0321, round-circle patterns

Squares to the Inch

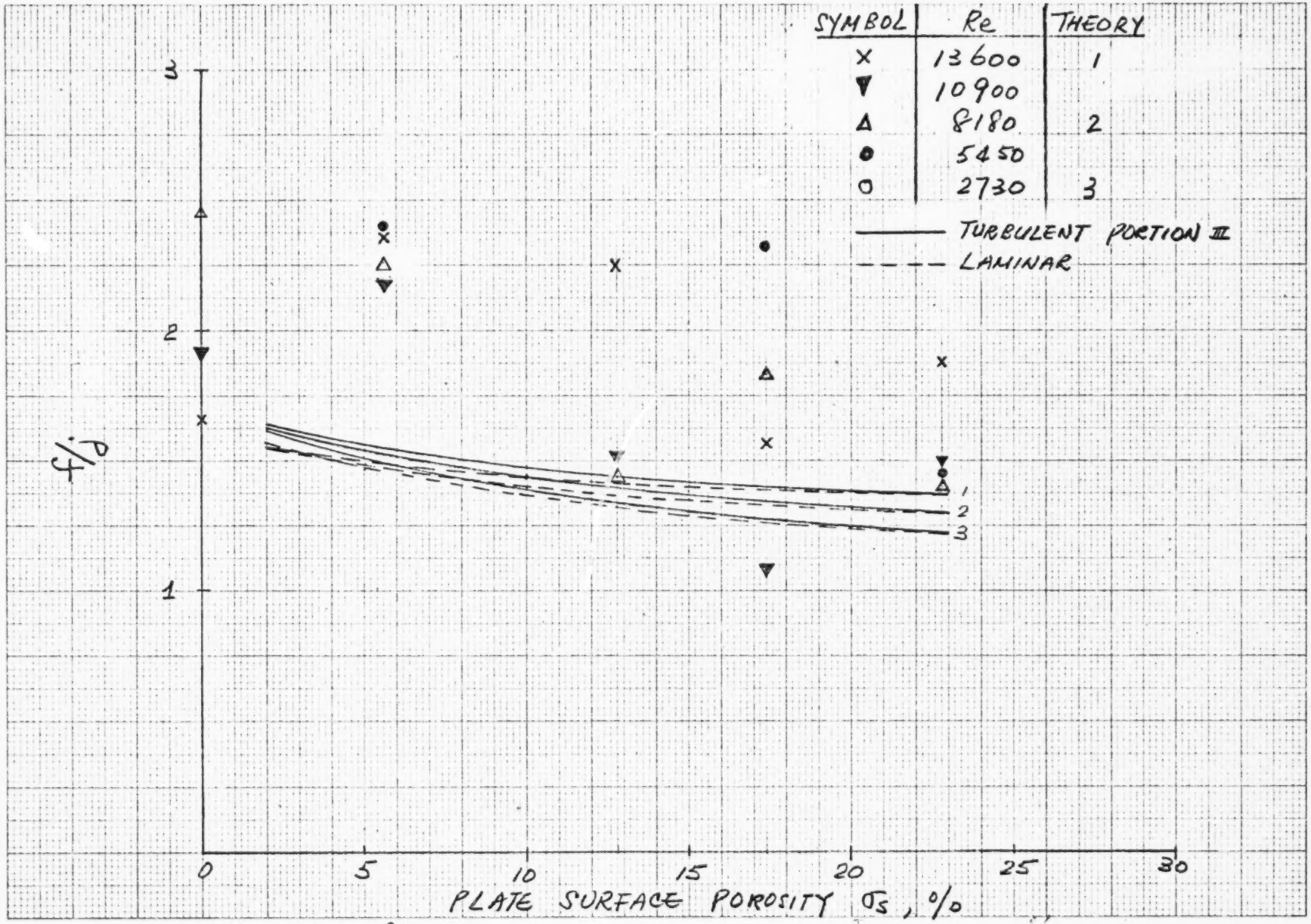

Fig 9c f/j vs σ_s for t/b=0.0321, round-circle patterns.

Squares to the inch

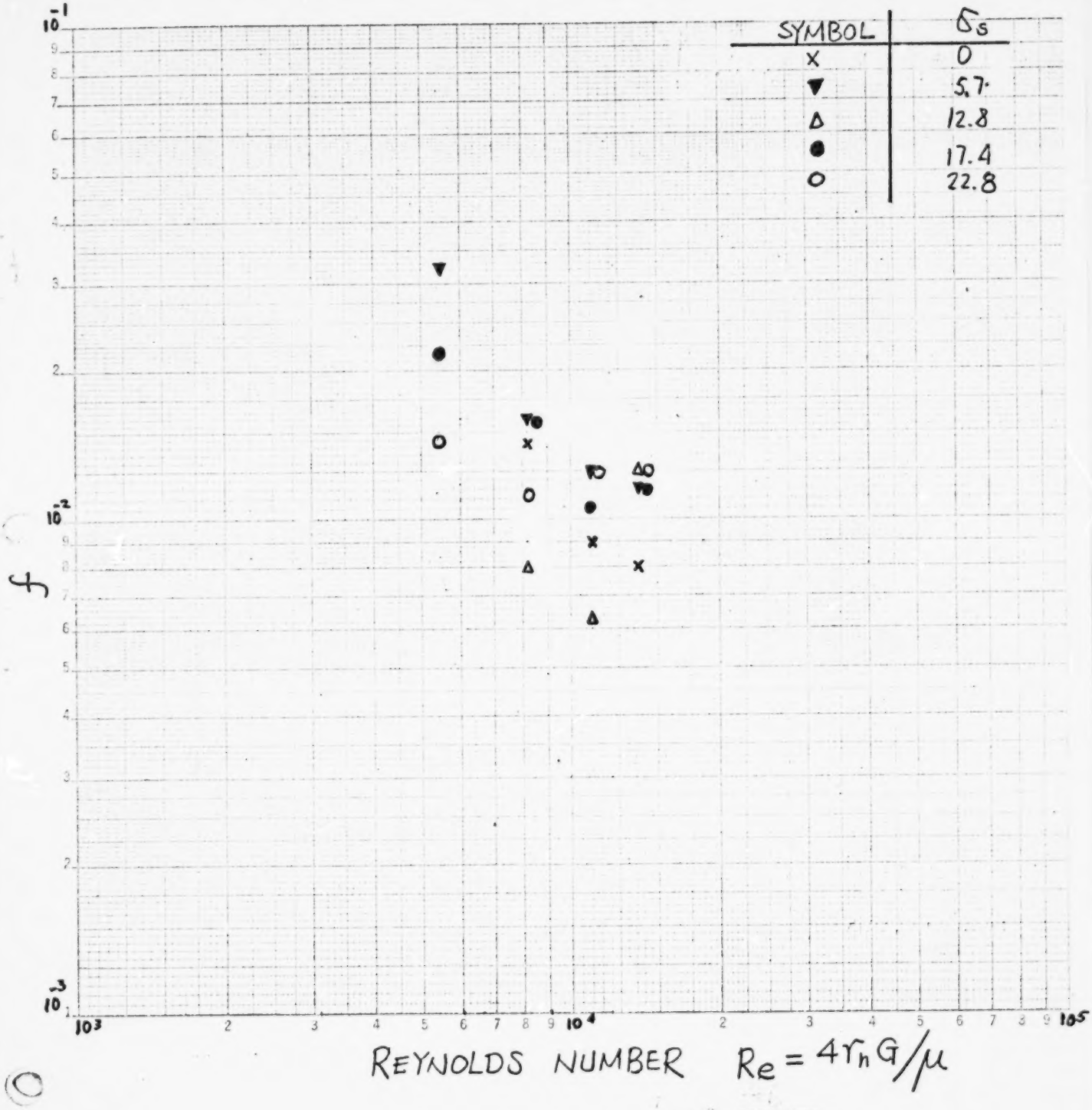

Fig 9d f vs Re for $t/b = 0.0321$, round-circle patterns

Logarithmic, 2 x 2 Cycles

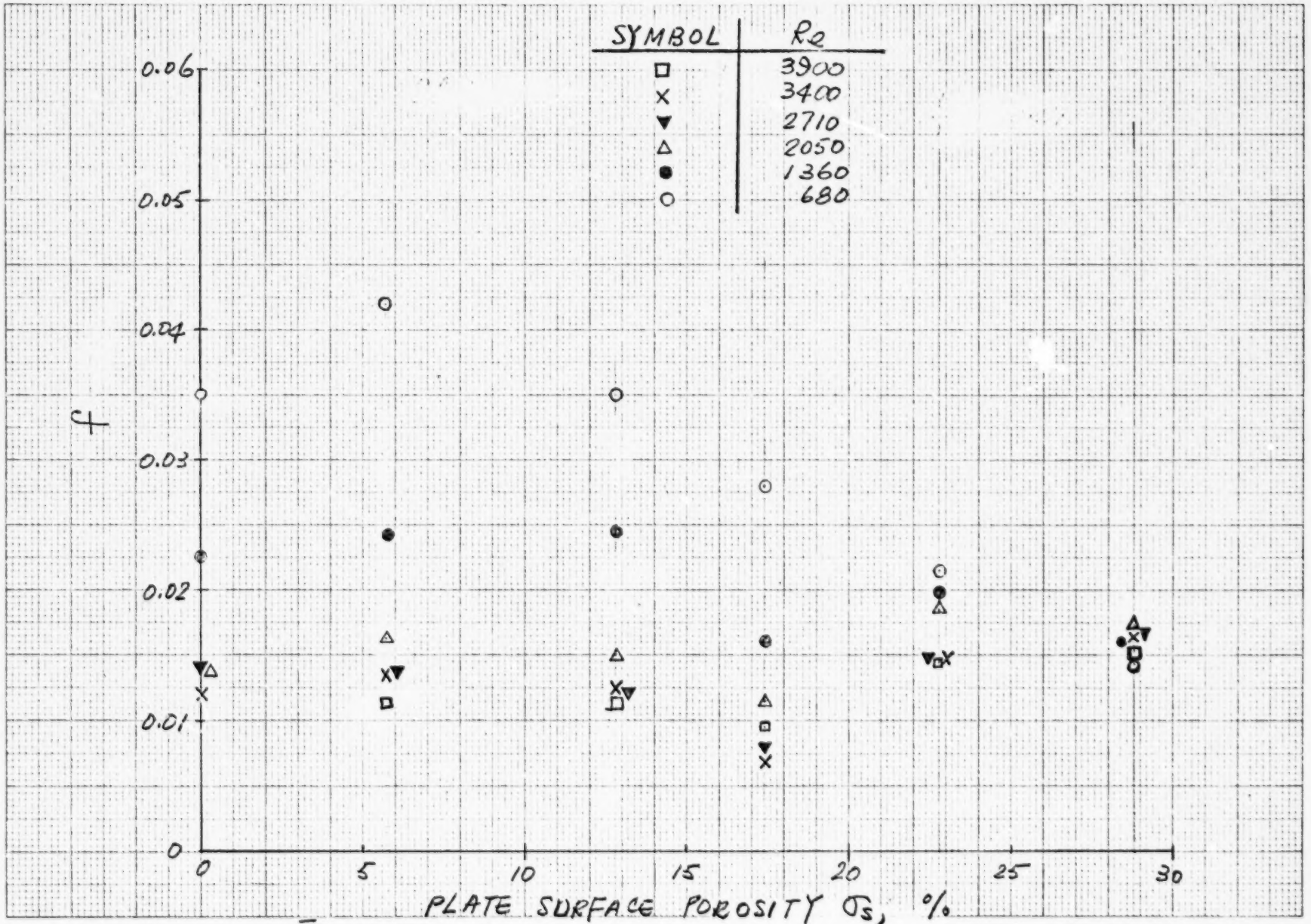

Fig 10 a f vs σ_s for t/b = 0.141, OVAL SLOTTED patterns

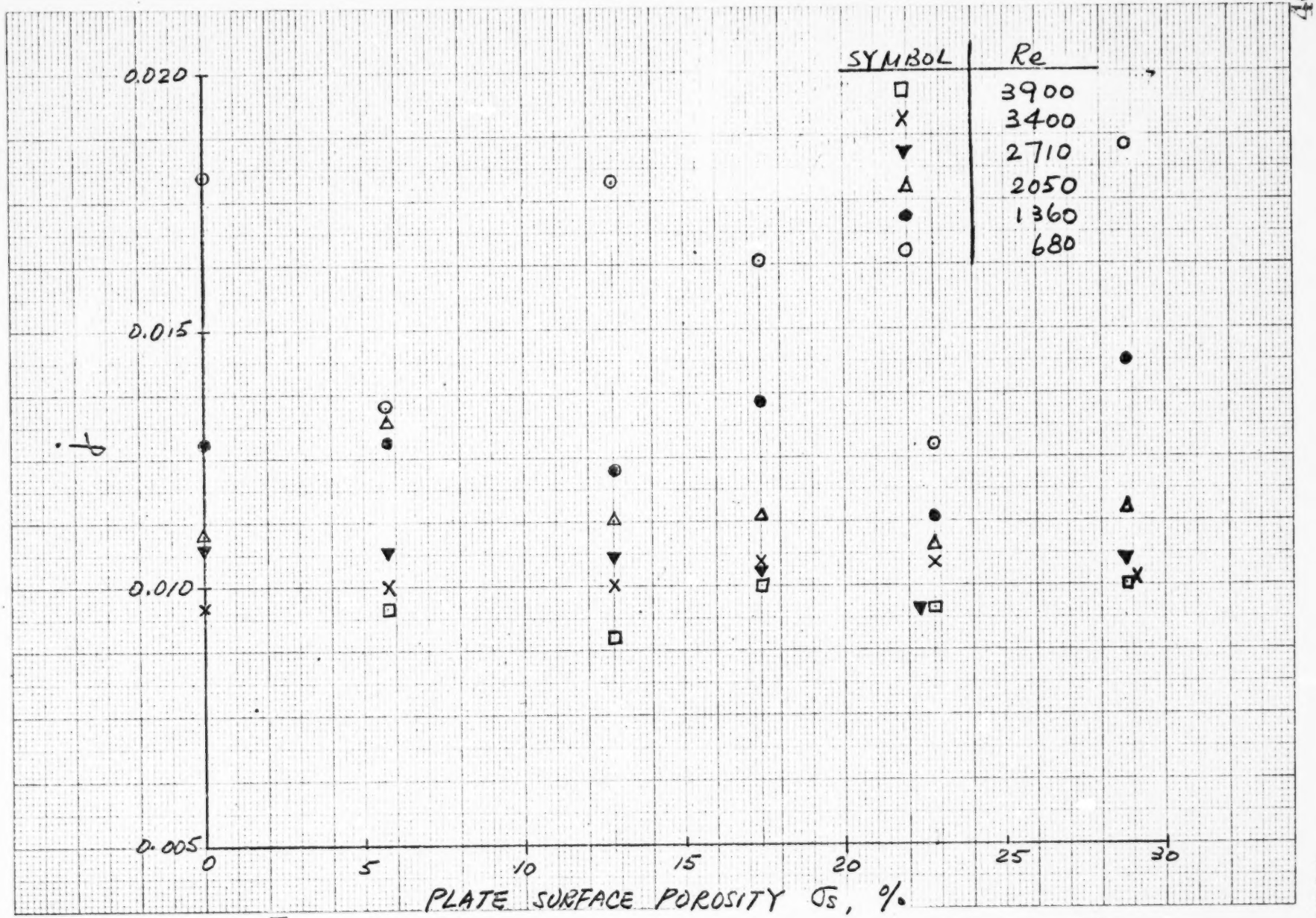

Fig 10b j vs σ_s for $t/b = 0.141$, OVAL SLOTTED patterns

' Squares to the Inch

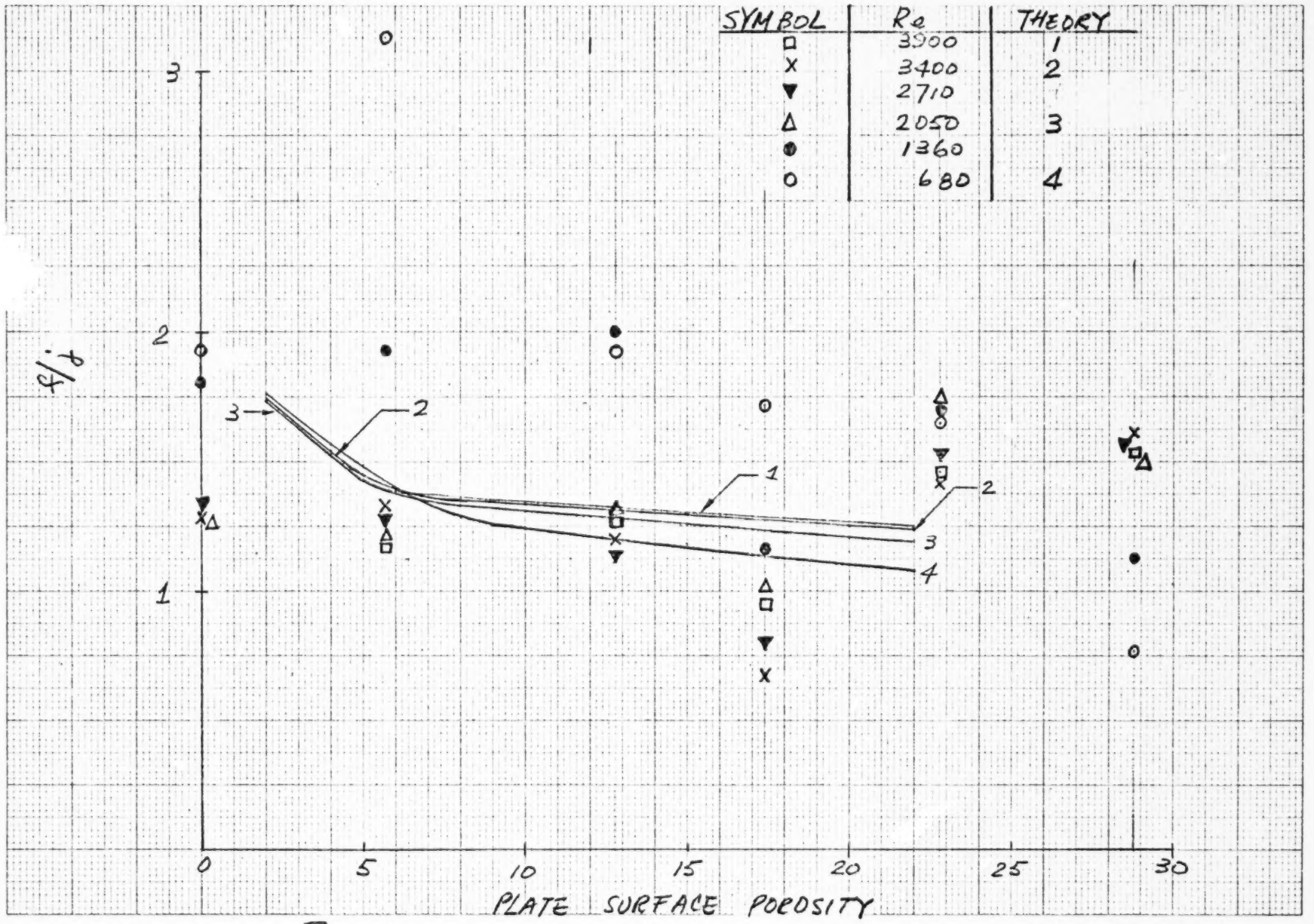

Fig 10 C f/j vs σ_s for t/b = 0.141, OVAL SLOTTED patterns

90 Squares to the Inch

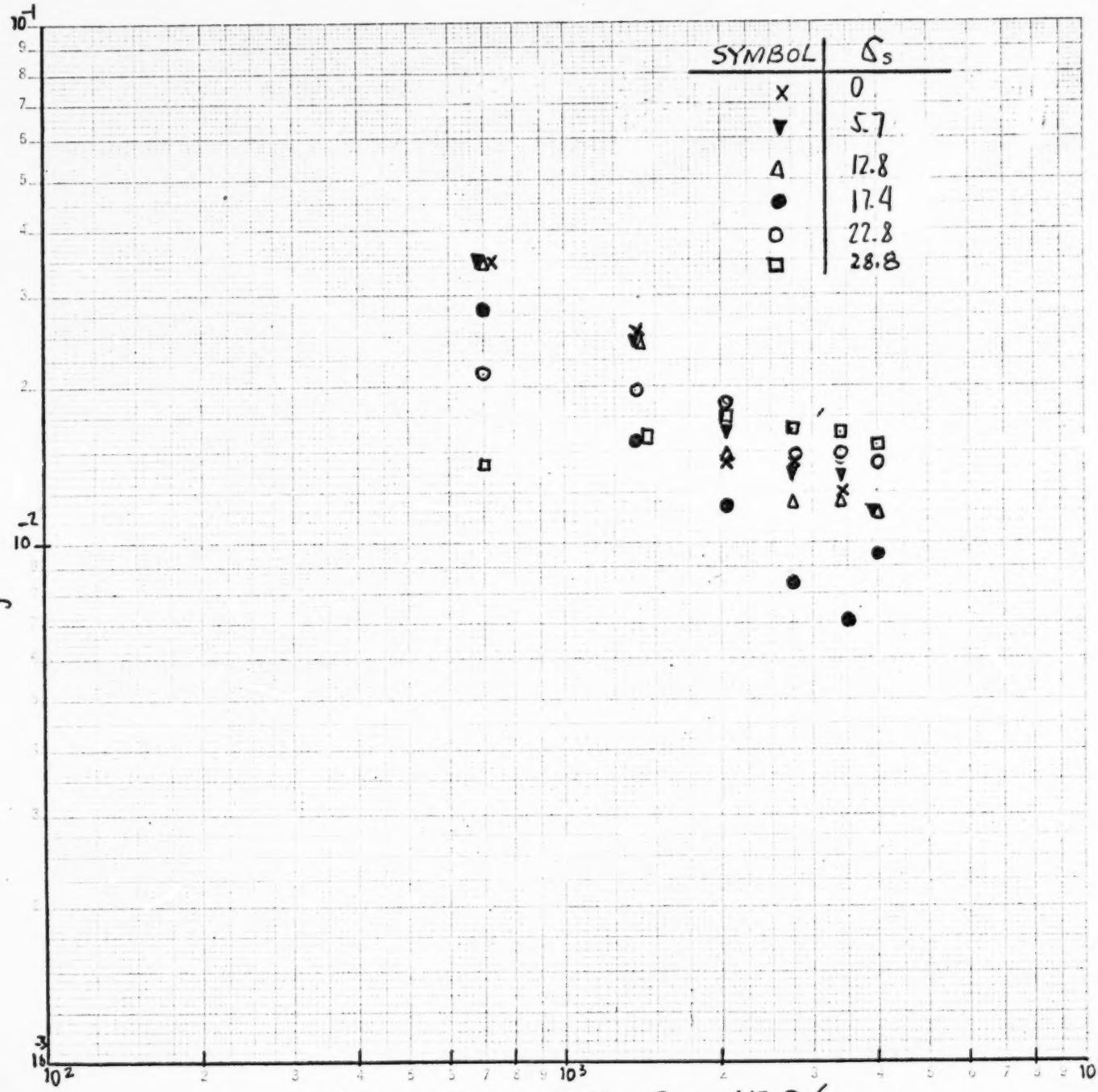

Fig. 10 d f vs Re for $t/b = 0.141$, oval-slotted patterns

arithmic, 2 x 2 Cycles

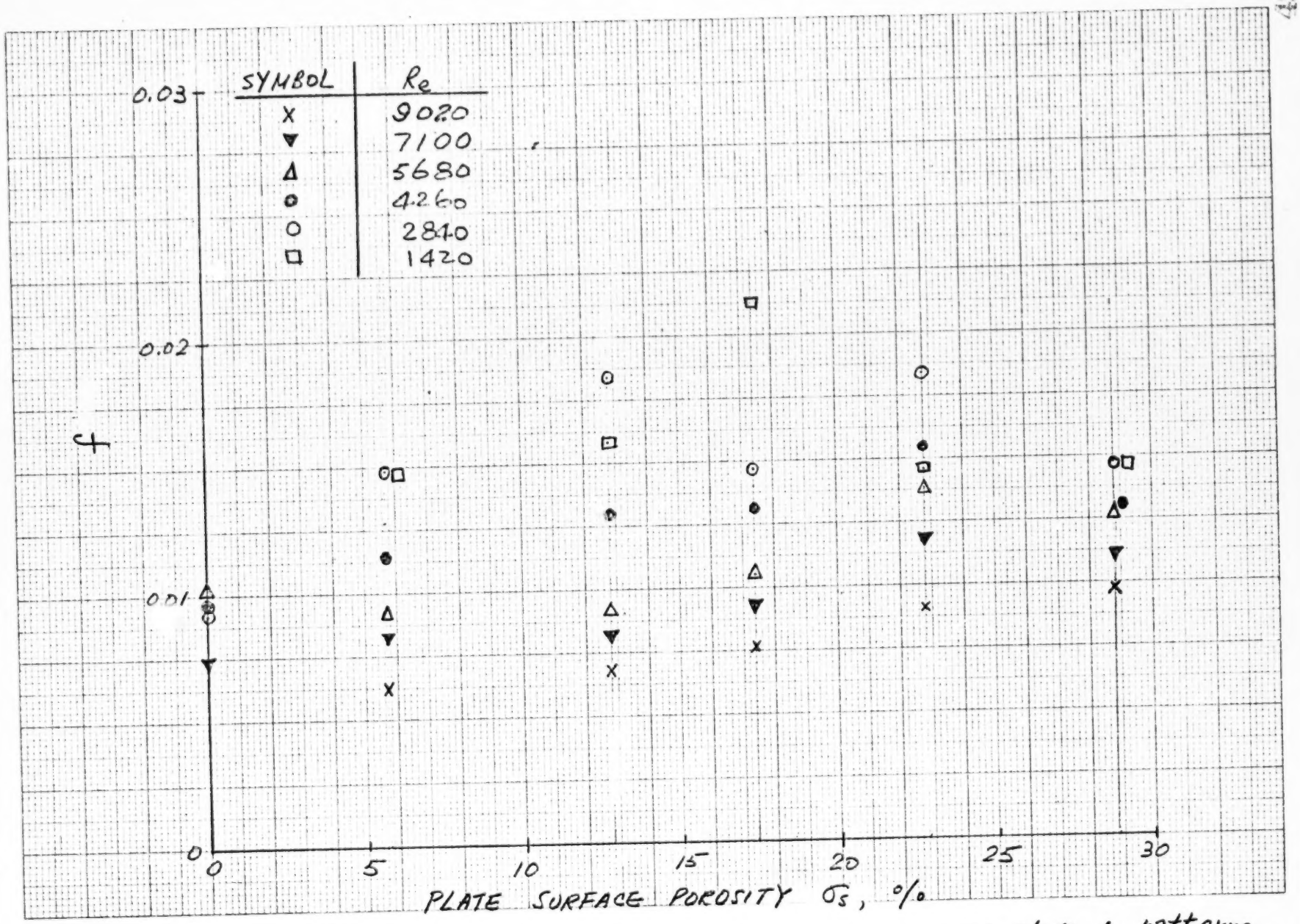

Fig 11a f vs σ_s for t/b = 0.0665, oval slotted patterns

Squares to the Inch

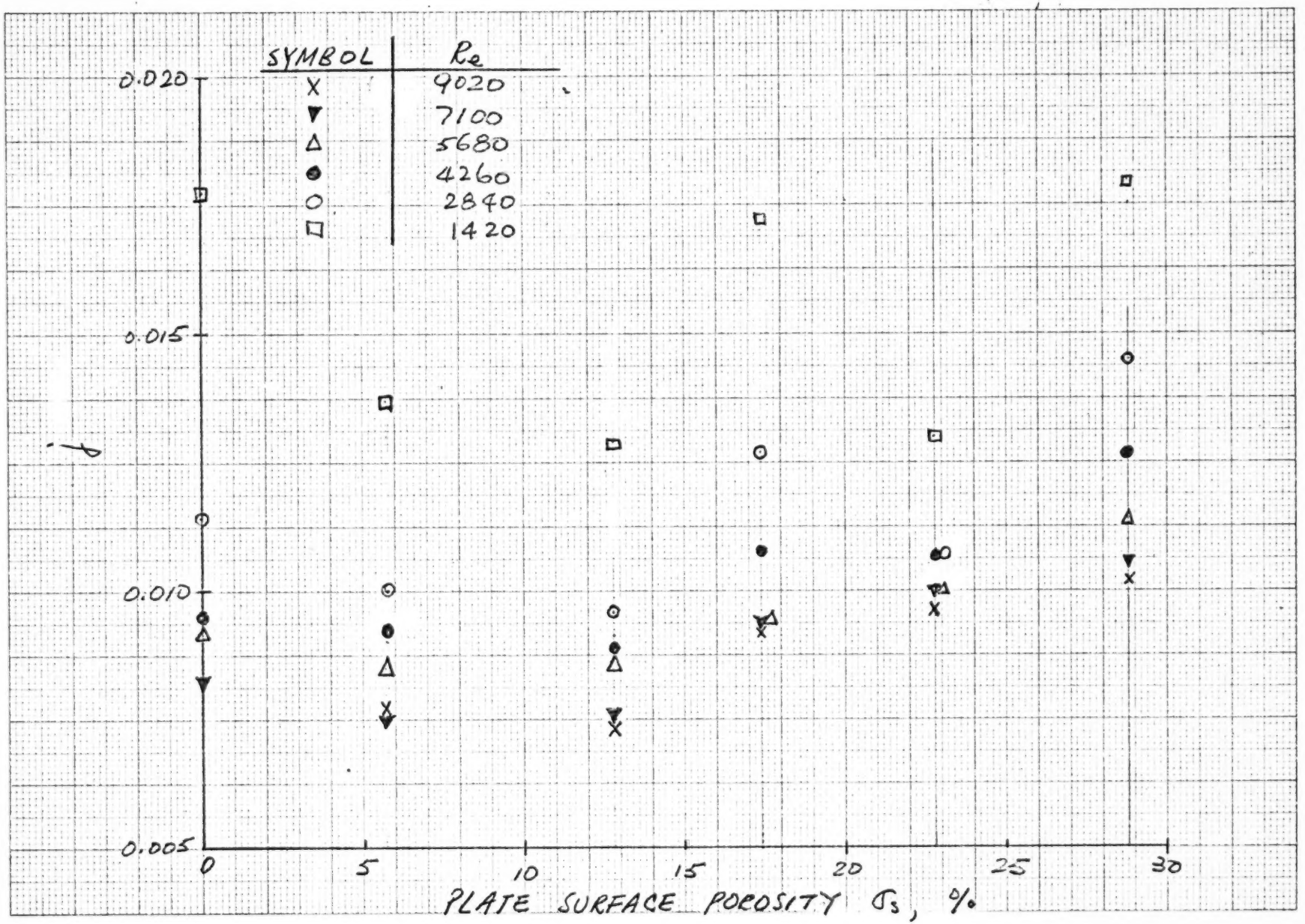

Fig 116 j vs σ_s for $t/b = 0.0665$, oval slotted patterns

Squares to the Inch

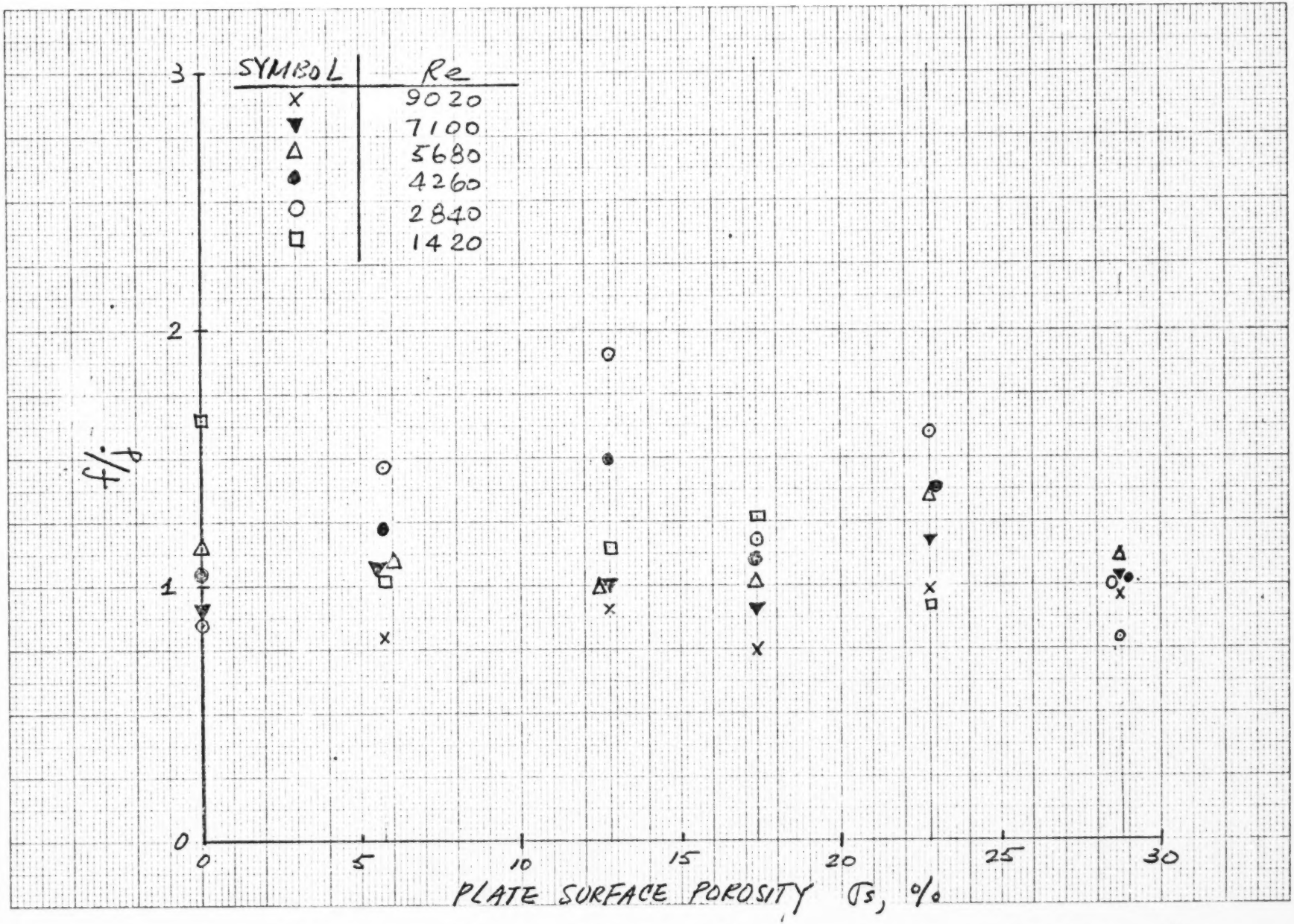

Fig 11c f/j vs σs for t/b = 0.0665, oval slotted patterns

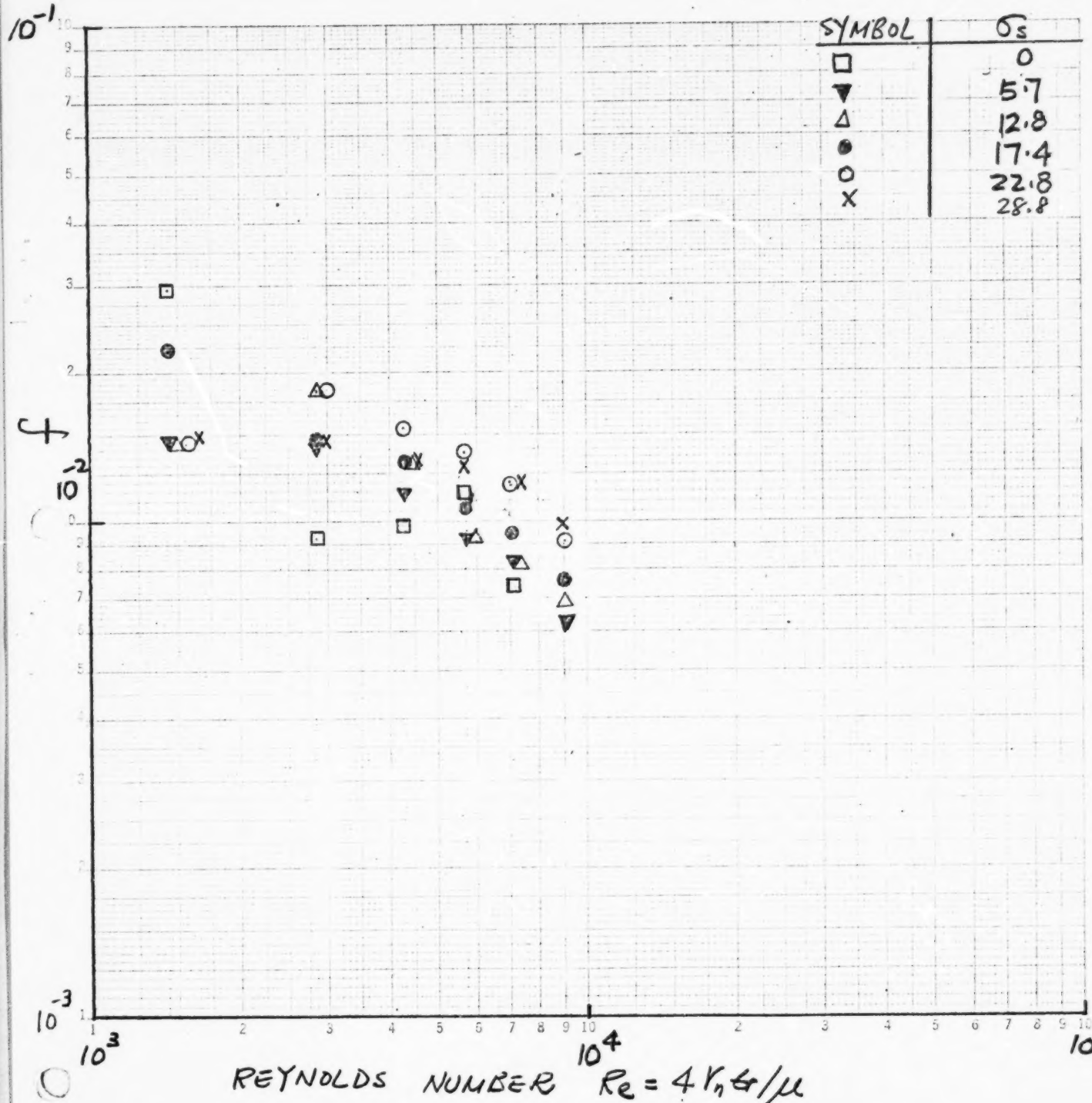

Fig 11 d f vs Re for $t/b = 0.0665$, oval slotted patterns

garithmic, 2 x 2 Cycles

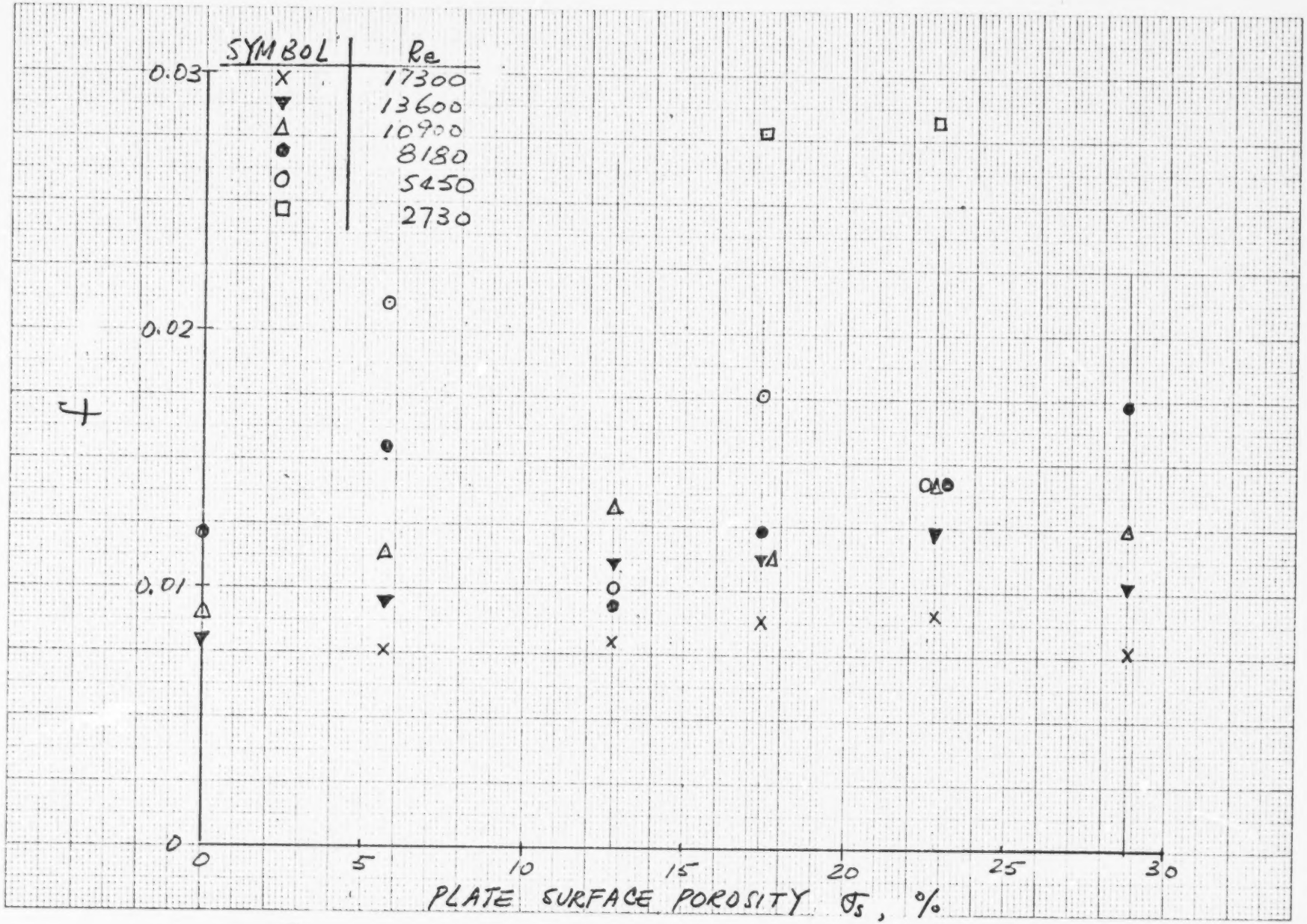

Fig 12 a f vs σ_s for $t/b = 0.0321$, oval slotted patterns

Squares to the Inch

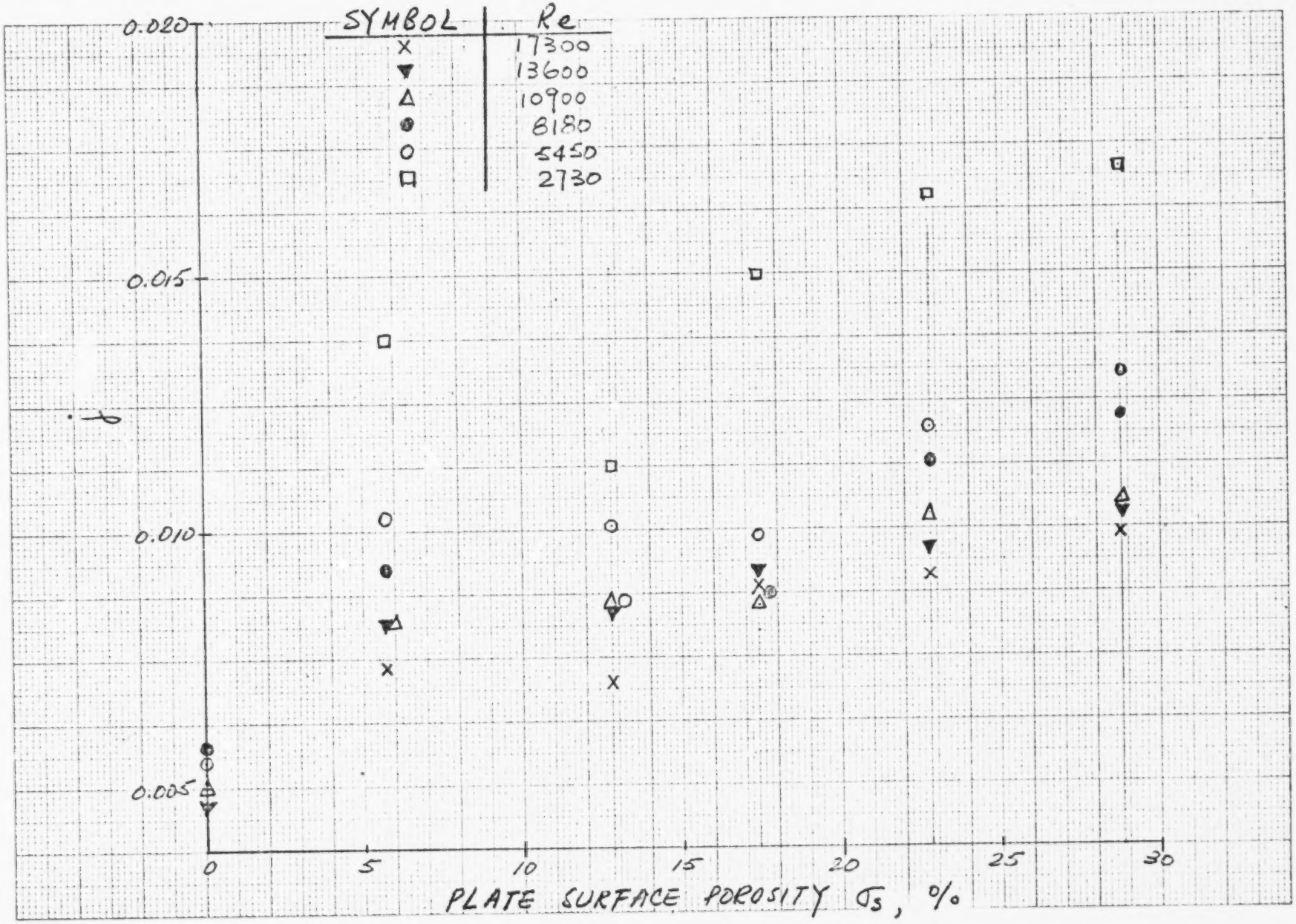

Fig 12 b j vs σ_s for t/b = 0.0321, oval slotted patterns

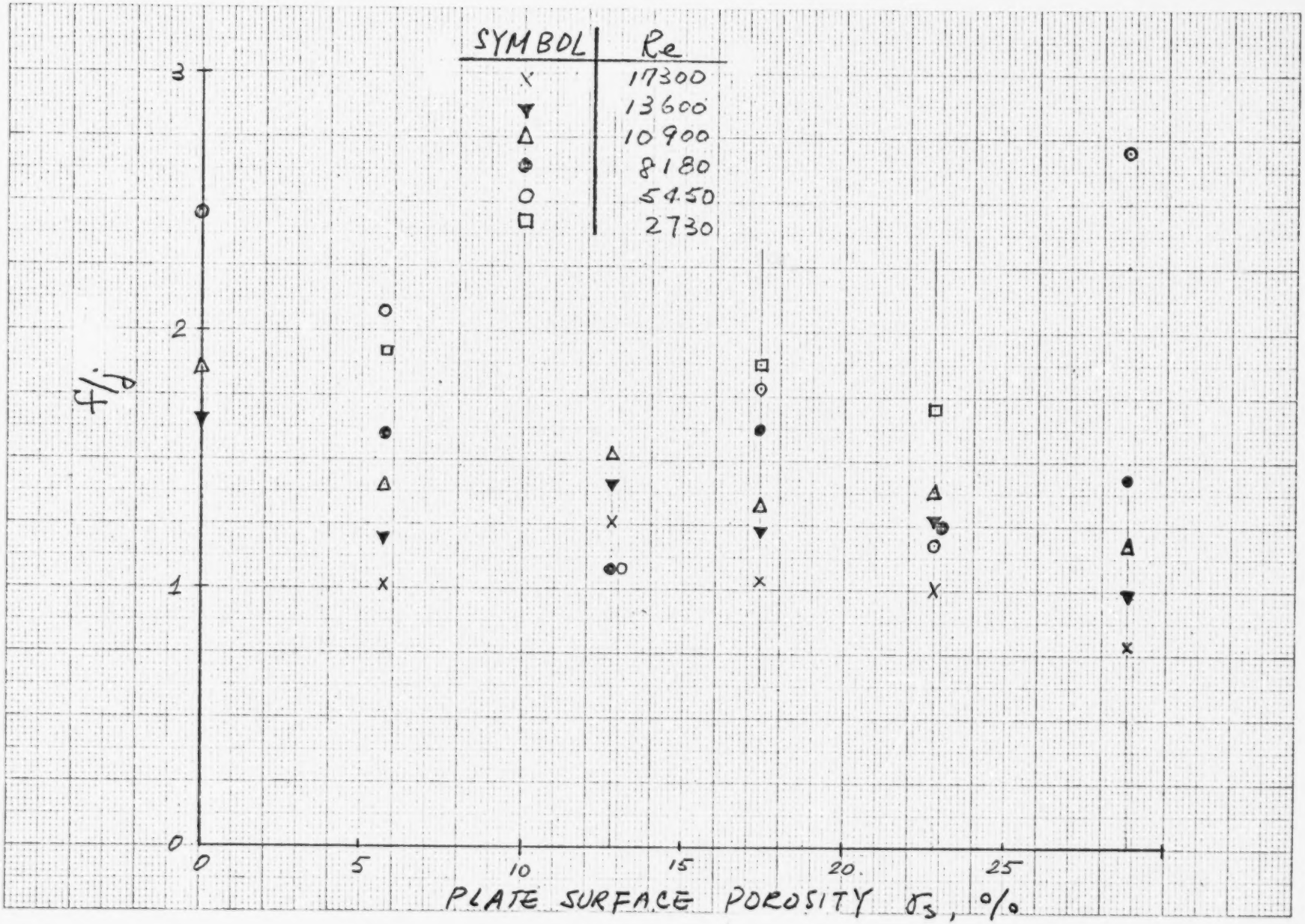

Fig 12c f/j vs σs for t/b = 0.0321, oval slotted patterns

Squares to the Inch

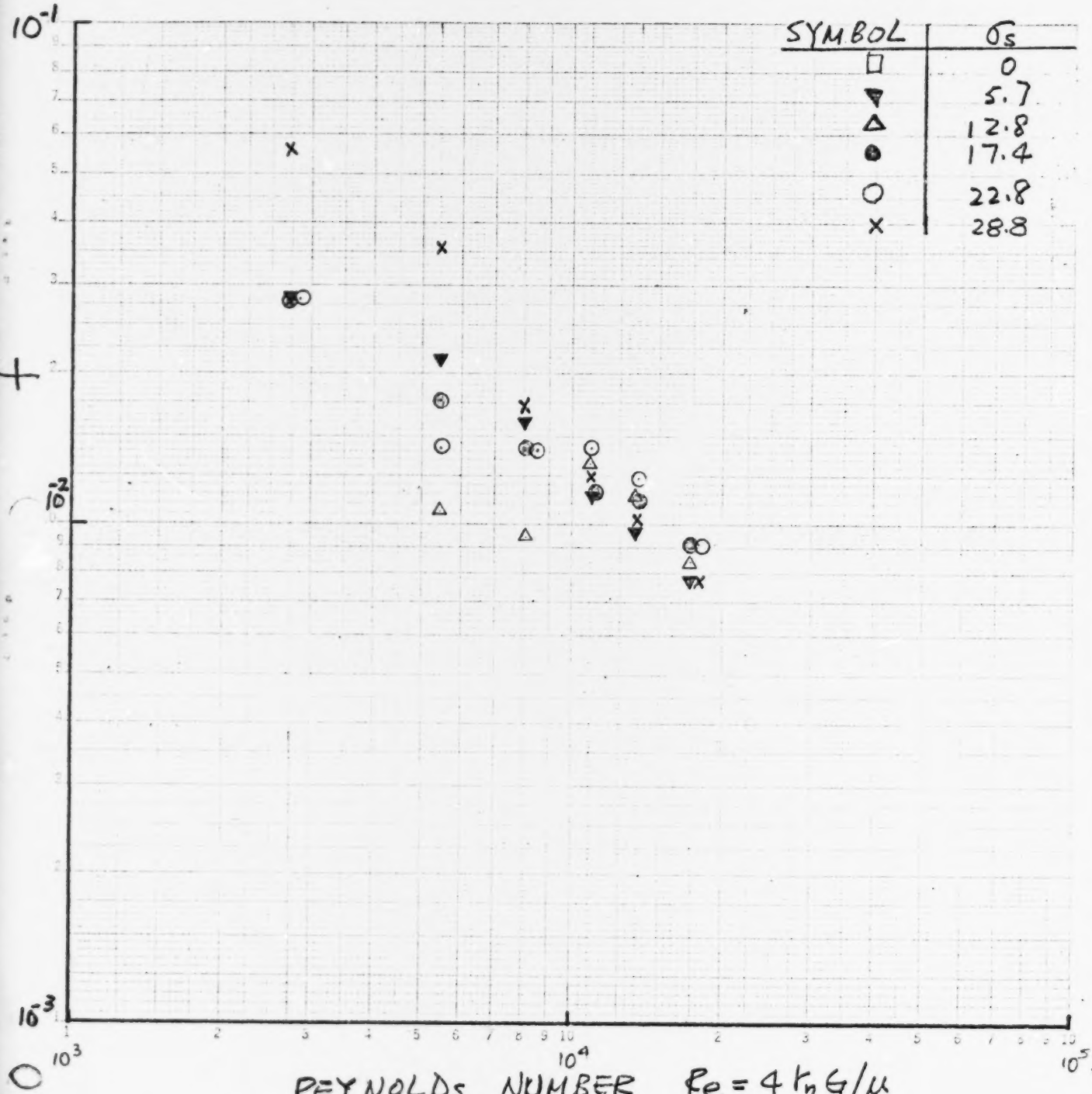

Fig 12d f vs Re for t/b = 0.0321, oval slotted pattern

arithmic, 2 x 2 Cycles

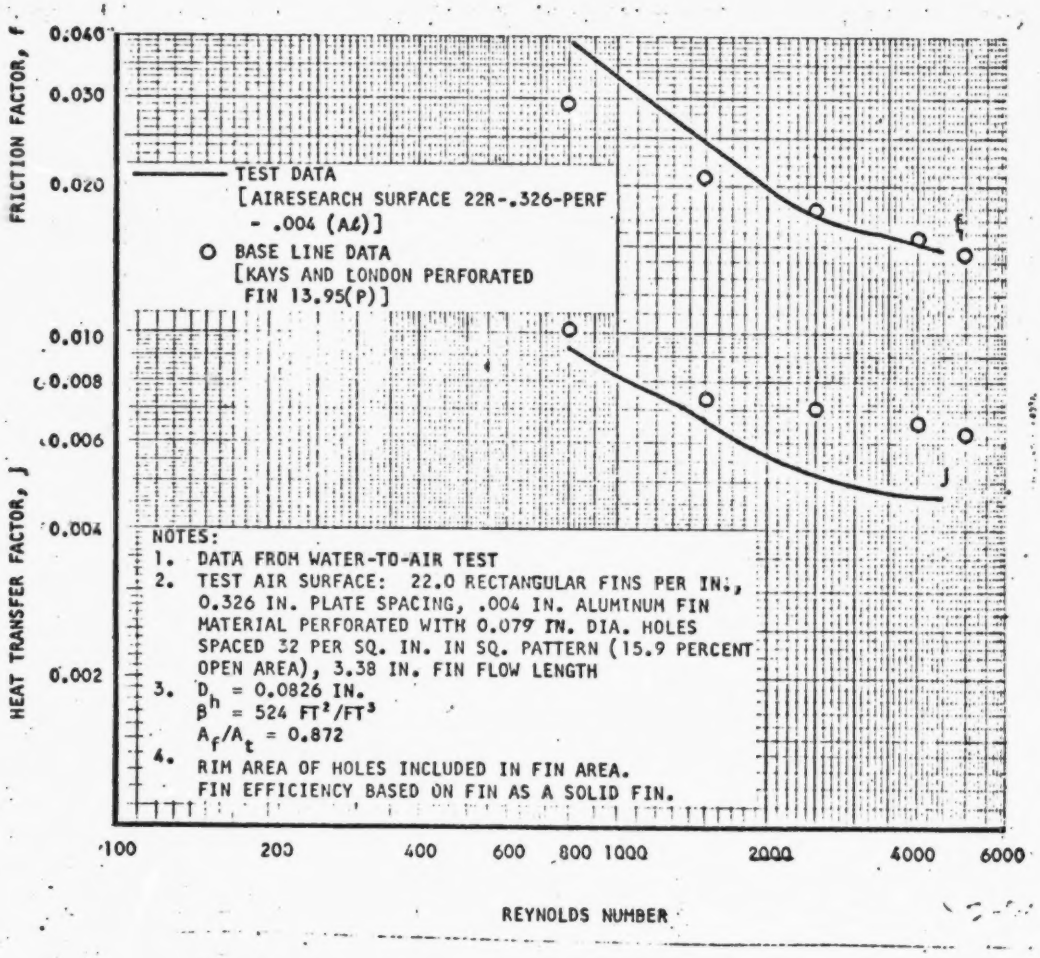

Figure 13. Performance Parameters 22 FPI Perforated Fin